*J. Fluid Mech.* (1996), *vol.* 323, *pp.* 339–365



# Viscous and inviscid instabilities of non-parallel self-similar axisymmetric vortex cores

By R. FERNANDEZ-FERIA

Universidad de Málaga, ETS Ingenieros Industriales, 29013 Málaga, Spain

(Received 3 January 1996)

A spectral collocation method is used to analyse the linear stability, both viscous and inviscid, of a family of self-similar vortex viscous cores matching external inviscid vortices with velocity $\boldsymbol{u}$ varying as a negative power of the distance $r$ to their axis of symmetry, $\boldsymbol{u} \sim r^{m-2}$ $(0 < m < 2)$. Non-parallel effects are shown to contribute at the same order as the viscous terms in the linear governing equations for the perturbations, and are consequently retained. The viscous stability analysis for the particular case $m = 1$, corresponding to Long's vortex, has recently been performed by Khorrami & Trivedi (1994). In addition to the inviscid non-axisymmetric modes of instability found by these authors, some inviscid axisymmetric unstable modes, and purely viscous unstable modes, both axisymmetric and non-axisymmetric, are also found. It is shown that, while both solution branches (I and II) of Long's vortex are destabilized by perturbations having negative azimuthal wavenumber $(n < 0)$, only the Type II Long's vortex is also unstable for axisymmetric disturbances $n = 0$, as well as for disturbances with $n > 0$. Global pictures of instabilities of Long's vortex are given. For $m > 1$, the vortex cores have the interesting property of losing existence when the swirl number is larger than an $m$-dependent critical value, in close connection with experimental results on vortex breakdown. The instability pattern for $m > 1$ is similar to that found for Long's vortex, but with the important difference that the parameter characterizing the different vortices, and therefore their stability, is a swirl parameter, which is precisely the one known to govern the real problem, while this is not the case in the highly degenerate case $m = 1$.

## 1. Introduction

The analysis of the linear stability of swirling flows, particularly of swirling jets, has been the subject of a number of works since the seminal one by Howard & Gupta (1962): Uberoi, Chow & Narain (1972), Lessen, Singh & Paillet (1974), Lessen & Paillet (1974), Duck & Foster (1980), Stewartson (1982), Leibovich & Stewartson (1983), Duck (1986), Khorrami (1991*a*), Mayer & Powell (1992), Duck & Khorrami (1992), Foster (1993), among others. Most of these investigations focused on Batchelor's (1964) trailing vortex solution. More directly related to the present work are those that analyse the temporal stability of Long's (1958, 1961) vortex, among them Foster and Duck (1982), Foster and Smith (1989), Foster and Jacqmin (1992), Khorrami and Trivedi (1994), Ardalan, Draper and Foster (1995). The spatial stability of Long's vortex has also been analysed recently by Drazin, Banks, and Zaturska (1995). Long's vortex, contrary to other columnar vortex models, is non-parallel: it has a small radial velocity component and the flow magnitudes present

a slow variation in the axial direction. This characteristic has made Long's vortex more suitable to model several types of high-Reynolds-number vortex cores, including tornadoes and other geophysical vortices, as well as vortices of technological interest, mainly in the fields of aeronautics and chemical engineering. The study of the stability of these model vortices, in addition to its theoretical interest, is thus important in the understanding and the ability to control swirling flows of technological and geophysical relevance.

This paper analyses the stability of a family of self-similar axisymmetric vortex cores which are exact solutions to the near-axis boundary layer approximation to the Navier–Stokes equations matching an external (inviscid) velocity $\boldsymbol{u}$ proportional to a negative power of the distance $r$ to the axis of symmetry, $\boldsymbol{u} \sim r^{m-2}$, where $m$ is in the range $0 < m < 2$. This family includes the well-known Long's vortex as the particular case $m = 1$. The structure of these vortices is described by Fernandez-Feria, Fernandez de la Mora & Barrero (1995, hereinafter referred to as FFB; see also §2 below). For $m \neq 1$, the core structure is solely dependent on the so-called *swirl parameter* $L$, or ratio of the inviscid near-axis swirl to axial velocity, there being two independent solutions for $L$ smaller (when $1 < m < 2$) or larger (when $0 < m < 1$) than a critical (or folding) value $L^*(m)$, and none otherwise. Thus, the set of three ordinary differential equations governing these vortices (see §2) has the interesting property of losing existence when the swirl parameter $L$ is larger (when $1 < m < 2$) or smaller (when $0 < m < 1$) than a critical value $L^*(m)$, a behaviour which supports the theory proposed by Hall and others (e.g. Hall 1972) on vortex breakdown. For $m = 1$ all the solutions have the same swirl number ($L = \sqrt{2}$), and the core structure is characterized by the axial flow force parameter $M$ (which is constant along the vortex only for $m = 1$; see Long 1961 and FFB): for values of $M$ larger than a critical value $M^*$ two independent solutions exist and none for $M < M^*$. However, since the parameter governing vortex breakdown for high-Reynolds-number real flows is found to be a swirl number (e.g. Spall, Gatski & Grosch 1987), and not a flow force, it was shown in FFB that viscous vortex cores may be modelled by the self-similar solutions with $m \neq 1$ (more precisely, $1 < m < 2$) better than by Long's vortex ($m = 1$). Indeed, the comparison made in FFB of both the critical swirl parameter and the viscous core structure for the family of self-similar vortices with several numerical and experimental results under conditions near the onset of vortex breakdown showed a good agreement for values of $m$ slightly larger than, but different from, unity.

The present study will analyse the linear stability, both viscous and inviscid, of the different solutions of the family of self-similar vortices for some values of $m > 1$ (particularly, the cases $m = 1.1$, whose structure is shown in FFB to agree fairly well with several experimental results for both confined and open vortex cores, and $m = 1.2$, are considered), and $m = 1$ (Long's vortex). One of the motivations is to investigate, in the light of the map of all the unstable modes, whether some relation exists between hydrodynamic instabilities and the solution breakdown. The subject is of interest because, as is well known, one of the theories proposed to explain the vortex breakdown phenomenon relates it to hydrodynamic instabilities (e.g. Lessen *et al.* 1974; see also the reviews by Hall 1972, Leibovich 1984, and Escudier 1988). Here we have a clear example where, for swirl numbers above a critical value, the near-axis boundary layer equations governing the viscous core of the vortex fail to have a solution, which is the view proposed by Hall and others to explain the vortex breakdown phenomenon. On the other hand, since these vortices are described by self-similar solutions, the linear stability analysis is relatively easy to perform in comparison with other viscous flows where vortex breakdown occurs (e.g.

the stability analysis performed by Gefgat, Bar-Yoseph & Solan 1996 for confined swirling flows).

In addition to its possible interest for the relation between vortex breakdown and linear instabilities, the paper is also a contribution to the existing knowledge on linear stability of swirling jets, which has a long tradition (see references given above). Of particular interest here is the paper by Khorrami & Trivedi (1994, hereinafter denoted by KT), which analyses the *viscous* stability of Long's vortex. In fact, the staggered spectral collocation technique used by these authors (developed by Khorrami 1991*b*) is the one used in the present work to solve the set of linear equations for the stability problem (§3). In addition, the results given by these authors will be compared with the present ones for the particular case $m = 1$ as a test of the numerical method (§4). It will be seen that the present results for $m = 1$ coincide exactly with those given by KT for non-axisymmetric disturbances and high Reynolds numbers. However, a fundamental disagreement is found for the axisymmetric modes: some axisymmetric unstable modes are found in this work which these authors failed to uncover. Indeed, we shall see that the main difference in the stability of the two types of vortices for a given value of $m$ occurs in relation to axisymmetric disturbances. In addition, we find purely viscous unstable modes, of the type reported by Khorrami (1991*a*) in relation to trailing line vortices, which were also not found by KT for Long's vortex. Finally, §5 presents results for $m$ slightly larger than unity, and all the results are summarized and discussed in §6.

## 2. The basic vortices

The vortices whose stability will be analysed are self-similar solutions to the near-axis boundary layer approximation of the steady, incompressible and axisymmetric Navier–Stokes equations, matching inviscid vortical flows with velocity and pressure fields proportional to a certain power of the distance $r$ to the axis of symmetry (see FFB). In cylindrical polar coordinates $(r, \theta, z)$, the velocity field $(U, V, W)$ and pressure $P$ of this external inviscid flow are

$$W = W_o r^{m-2}, \quad U = 0, \quad V = \pm L W_o r^{m-2}, \quad \frac{P}{\rho} = \frac{(LW_o)^2}{2(m-2)} r^{2(m-2)}, \tag{2.1}$$

where $\rho$ is the fluid density, $0 < m < 2$, and $W_o$ and the swirl parameter $L$ are positive constants. The vortex core structure is given by

$$\Psi = \nu z f(\xi), \tag{2.2}$$

$$V = \frac{\nu z}{\delta^2(z)} \gamma(\xi), \quad \frac{P}{\rho} = \frac{(\nu z)^2}{\delta^4(z)} \beta(\xi), \tag{2.3}$$

where $\Psi$ is the stream function for the meridional motion, in terms of which the axial and radial velocity components are:

$$W = \frac{1}{r} \frac{\partial \Psi}{\partial r} = \frac{\nu z}{\delta^2(z)} 2 f'(\xi), \tag{2.4}$$

$$U = -\frac{1}{r} \frac{\partial \Psi}{\partial z} = -\frac{\nu}{r} \left[ f(\xi) - \frac{2\xi f'(\xi)}{m} \right]. \tag{2.5}$$

In the above expressions, $\delta(z)$ is the boundary layer thickness,

$$\delta(z) = \left(\frac{mvz}{W_o}\right)^{1/m}, \tag{2.6}$$

and the similarity variable $\xi$ is defined by

$$\xi \equiv \eta^2, \quad \eta = \frac{r}{\delta(z)}. \tag{2.7}$$

The functions $f, \gamma$ and $\beta$ are governed by the following set of nonlinear ordinary differential equations:

$$\gamma^2 = 2\xi\beta', \tag{2.8}$$

$$2\frac{m-1}{m}\gamma f' - 2f\gamma' - \frac{f\gamma}{\xi} = 4(\xi\gamma')' - \frac{\gamma}{\xi}, \tag{2.9}$$

$$\frac{2-m}{m}f'^2 + ff'' + \frac{1}{2m}[(2-m)\beta + \xi\beta'] = -2(\xi f'')', \tag{2.10}$$

where the primes denote differentiation with respect to $\xi$. These equations are solved in FFB subject to regularity conditions at the axis,

$$\xi \to 0, \quad f = A_1\xi + o(\xi^2), \quad \gamma \pm A_2\xi^{1/2} + o(\xi^{3/2}), \quad \beta = -1 + o(\xi), \tag{2.11}$$

where $A_1$ and $A_2$ are arbitrary constants, and on matching with (2.1) as $\xi \to \infty$:

$$f \to (C\xi)^{m/2}, \quad \gamma \to \pm B\xi^{(m-2)/2}, \quad \beta \to \frac{B^2}{2(m-2)}\xi^{m-2}, \tag{2.12}$$

$$B = mLC^{m/2}. \tag{2.13}$$

As discussed in FFB, owing to the invariance of (2.8)–(2.10) under the uniparametric group of transformation of scale $f \to f$, $\xi \to C\xi$, $\gamma \to \gamma/C$, $\beta \to \beta/C^2$, one may start the numerical integration of these equations with just two degrees of freedom, $A_1$ and $A_2$, choosing $-1$ as the pressure constant at the axis (equation (2.11)). The scaling constant $C$ is then obtained numerically (equation (2.12)), as well as the constant $B$ which fixes the swirl parameter $L$ through (2.13). However, as shown in FFB, the two constants $A_1$ and $A_2$ are not independent, but for each $A_1$ in the interval $-1/\sqrt{2} < A_1 < \infty$ (note that $A_1$ is related to the axial velocity at the axis through $\delta^2 W(r=0)/(vz) = 2f'(0) = 2A_1$), the desired behaviour (2.12) at infinity requires finding a certain value $A_2(A_1)$, which is obtained by shooting. As a consequence, for each $m$, the swirl parameter $L$ is a function of $A_1$. Except for the case $m = 1$, this function is non-monotonic, having an extremum $L^*(m)$, which is a minimum for $0 < m < 1$ and a maximum for $1 < m < 2$ (see figures 2 and 3 in FFB). Thus, when $0 < m < 1$, two solutions exist for $L > L^*(m)$, and there is no solution for $L < L^*(m)$; when $1 < m < 2$, no solutions exist for $L > L^*(m)$, and there are two possible solutions for $L < L^*(m)$. For the special case $m = 1$, which corresponds to Long's vortex, $L = \sqrt{2}$ for all values of $A_1$. In this particular case, the non-dimensional flow force parameter, $M$, which is constant along the axis for $m = 1$,

$$M = \frac{\pi}{B^2}\int_o^\infty (\beta + 4f'^2)\mathrm{d}\xi \quad (m = 1), \tag{2.14}$$

plays a role somewhat analogous to $L$ for $m \neq 1$ (Long 1961; Burggraf & Foster 1977): for $M > M^* \simeq 3.75$ two solutions exist (denoted by Burggraf & Foster as Type I and Type II solutions) and none for $M < M^*$.

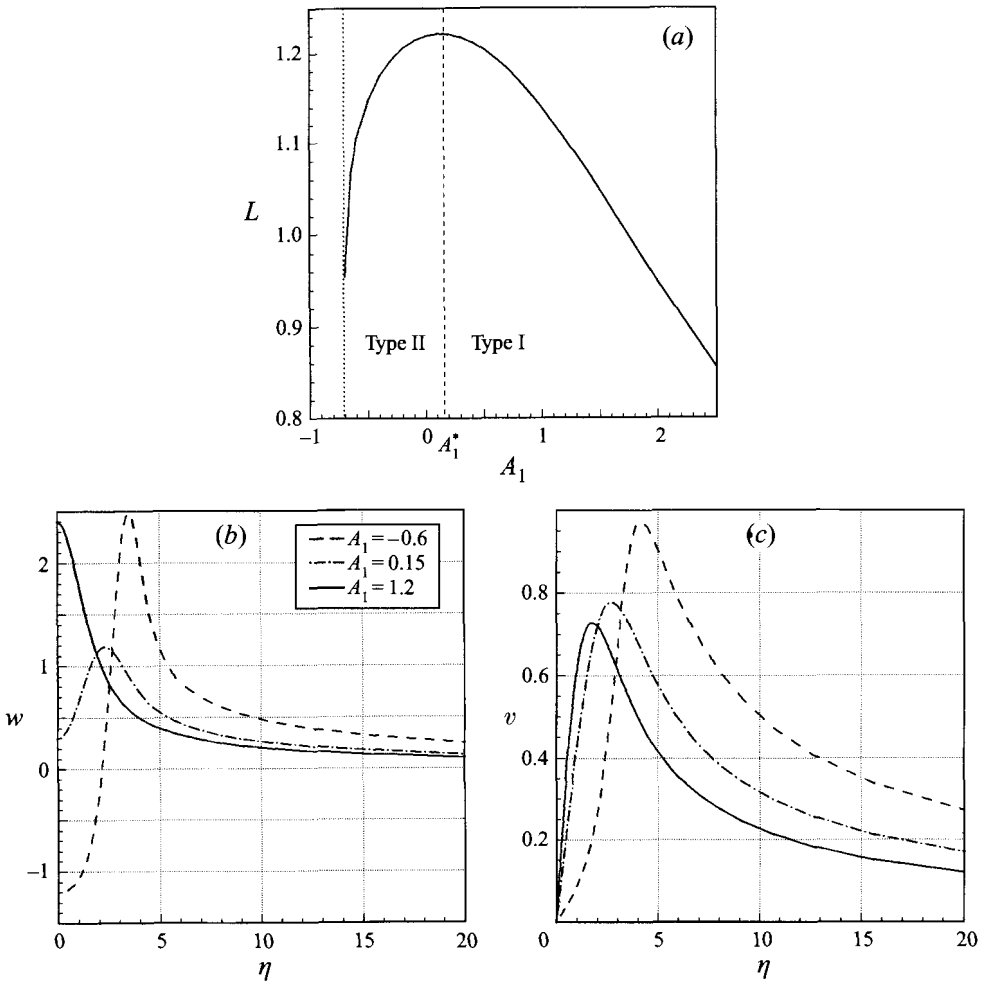


FIGURE 1. Basic vortices for $m = 1.1$. (*a*) Function $L(A_1)$. The folding or critical value of $L$ is $L^* \simeq 1.223$ ($A_1^* \simeq 0.15$ and $A_2 \simeq 0.45$). Two different solutions exist for $L < L^*$ (Type I for $A_1 > A_1^*$ and Type II for $-1/\sqrt{2} < A_1 < A_1^*$), and none for $L > L^*$. (*b,c*) Axial and azimuthal velocity profiles for different values of $A_1$ (note that the axial velocity at the axis is $2A_1$.) Although only the interval $0 \leqslant \eta \leqslant 20$ is plotted, $\eta_{max} = 50$ is used in all the computations.

As mentioned in the Introduction, it was shown in FFB that from a physical point of view the most interesting velocity profiles of the family are those corresponding to values of $m$ slightly larger than unity. For that reason, $m = 1.1$ and $m = 1.2$ have been chosen for the stability analysis of §5. Figure 1 shows the function $L(A_1)$ and some axial and azimuthal velocity profiles for $m = 1.1$. By analogy with the notation of Burggraf & Foster, solutions are termed Type I or Type II depending on whether $A_1$ is in the interval $(A_1^*(m), \infty)$ or $(-1/\sqrt{2}, A_1^*(m))$, respectively. Prior to that, §4 considers the case $m = 1$ (Long's vortex), with the main motivations of comparing the present results with those obtained in previous works (especially KT), and providing a more complete map of the unstable regions for Long's vortex. The function $M(A_1)$ and some axial and azimuthal velocity profiles for $m = 1$ are depicted in figure 2.

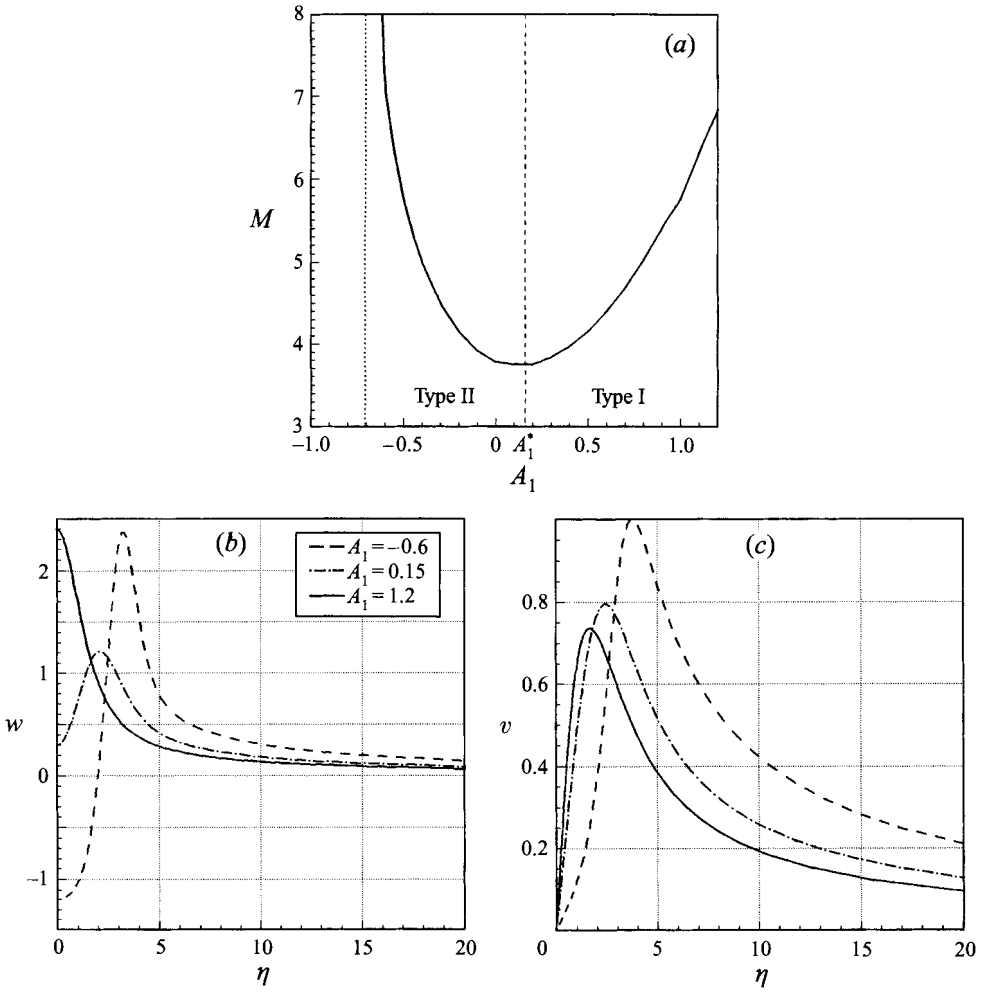


FIGURE 2. Long's vortex ($m = 1$). ($a$) Function $M(A_1)$. The critical (folding) value is $M^* \simeq 3.75$ ($A_1^* \simeq 0.15$ and $A_2 \simeq 0.50$). ($b$,$c$) Axial and azimuthal velocity profiles for different values of $A_1$.

## 3. Stability formulation and numerical method

To study the linear stability of the above-described family of swirling jets, the flow variables, $(u, v, w)$ and $p$, are decomposed, as usual, into a mean part, $(U, V, W)$ and $P$, and a small perturbation. After (2.3)–(2.5),

$$w = \frac{vz}{\delta^2}[2f' + \overline{w}], \quad u = \frac{v}{r}\left[-f + \frac{2\xi f'}{m} + \frac{rz}{\delta^2}\overline{u}\right], \tag{3.1}$$

$$v = \frac{vz}{\delta^2}[\gamma + \overline{v}], \quad \frac{p}{\rho} = \frac{(vz)^2}{\delta^4}[\beta + \overline{p}]. \tag{3.2}$$

The small dimensionless fluctuating velocity and pressure fields, $(\overline{u}, \overline{v}, \overline{w})$ and $\overline{p}$, are assumed to be of the form

$$[\overline{u}, \overline{v}, \overline{w}, \overline{p}] = [\mathrm{i}F(\xi), G(\xi), H(\xi), \Pi(\xi)]\mathrm{e}^{\mathrm{i}(kz + n\theta - \Omega t)}, \tag{3.3}$$

where $F, G, H$ and $\Pi$ are the complex eigenfuctions, $n$ is the azimuthal wavenumber, and $k$ and $\Omega$ are the dimensional axial wavenumber and frequency, respectively. Note that, as a difference with KT, the scaling factors multiplying both the dimensionless mean flow and perturbations in (3.1) and (3.2) are $z$-dependent. Also, the amplitudes $F$, $G$, $H$ and $\Pi$ are assumed to be functions of the self-similar variable $\xi$, instead of just the radial distance $r$. All this will allow the rate of change in the axial direction of the basic flow and the amplitude of the perturbations to be taken into account. It should also be noted that, although other ways of taking normal modes are possible, the form (3.1)–(3.3) does not restrict the admissible class of perturbations, so that general linearized perturbations are considered.

As shown below, the axial wavelengths of interest are of the order of (or larger than) the boundary layer thickness. Accordingly, the following dimensionless, order of unity (or smaller), local axial wavenumber will be used instead of $k$:

$$\alpha \equiv \delta k. \tag{3.4}$$

The corresponding local dimensionless frequency is

$$\omega \equiv \frac{\delta^3 \Omega}{z\nu}. \tag{3.5}$$

For the analysis of temporal stability performed here, the axial wavenumber $\alpha$ will be taken to be real and non-negative, and the frequency $\omega$ will be complex. Depending on the sign of the imaginary part of the frequency, $\omega_i$, the perturbations will be either growing (unstable) or decaying (stable) in time.

Substituting (3.1)–(3.5) into the Navier–Stokes equations for the steady flow of an incompressible fluid, and neglecting second-order terms in both the small perturbations and the inverse of the local Reynolds number,

$$\Delta \equiv \frac{\delta}{z} = \left(\frac{m\nu}{W_o}\right)^{1/m} z^{(1-m)/m} \equiv Re^{-1}, \tag{3.6}$$

which is assumed to be small within the boundary layer approximation, the following set of linear equations results:

continuity

$$(\xi^{1/2}F)' + \frac{n}{2}\frac{G}{\xi^{1/2}} + \frac{\alpha}{2}H + \frac{\Delta}{2\mathrm{i}}\left[\frac{m-2}{m}H - \frac{2\xi}{m}H'\right] = 0; \tag{3.7}$$

$r$-momentum

$$-4\mathrm{i}\Delta\xi F'' - 2\mathrm{i}\Delta(f+2)F' + \left[\omega - \frac{n\gamma}{\xi^{1/2}} - 2\alpha f' + \mathrm{i}\Delta\left(\frac{1+f}{\xi} - \frac{2}{m}f' + \frac{4\xi f''}{m} + \frac{n^2}{\xi} + \alpha^2\right)\right]F$$

$$- \frac{2}{\xi^{1/2}}\left(\gamma - \mathrm{i}\Delta\frac{n}{\xi^{1/2}}\right)G + 2\xi^{1/2}\Pi' = 0; \tag{3.8}$$

$\theta$-momentum

$$-4\Delta\xi G'' - 2\Delta(f+2)G' + \left[-\mathrm{i}\omega + \frac{\mathrm{i}n\gamma}{\xi^{1/2}} + 2\mathrm{i}\alpha f' + \Delta\left(\frac{2(m-1)}{m}f' + \frac{1-f}{\xi} + \frac{n^2}{\xi} + \alpha^2\right)\right]G$$

$$+ \left[2\mathrm{i}(\xi^{1/2}\gamma)' + \Delta\frac{2n}{\xi}\right]F + \frac{\mathrm{i}n}{\xi^{1/2}}\Pi + \Delta\left(\frac{m-2}{m}\gamma - \frac{2\xi}{m}\gamma'\right)H = 0; \tag{3.9}$$

$z$-momentum

$$-4\Delta\xi H''-2\Delta(f+2)H'+\left[-\mathrm{i}\omega+\frac{\mathrm{i}n\gamma}{\xi^{1/2}}+2\mathrm{i}\alpha f'+\Delta\left(4\frac{(m-2)}{m}f'-\frac{4\xi}{m}f''+\frac{n^2}{\xi}+\alpha^2\right)\right]H$$

$$+4\mathrm{i}\xi^{1/2}f''F+\left[\mathrm{i}\alpha+\Delta\frac{2(m-2)}{m}\right]\Pi-\Delta\frac{2\xi}{m}\Pi'=0. \tag{3.10}$$

The boundary conditions are (Batchelor & Gill 1962; Khorrami 1991*b*):

$\xi\to\infty$

$$F(\infty)=G(\infty)=H(\infty)=0; \tag{3.11}$$

$\xi=0$

$$F(0)=G(0)=0,\quad H'(0)=0,\quad (n=0), \tag{3.12}$$

$$F(0)\pm G(0)=0,\quad F'(0)=0,\quad H(0)=0\quad (n=\pm1), \tag{3.13}$$

$$F(0)=G(0)=H(0)=0\quad (|n|>1). \tag{3.14}$$

For $\Delta=0$ (inviscid problem), $m$ does not enter explicitly into (3.7)–(3.10), but through the mean-flow solutions. Therefore, equations (3.7)–(3.10) coincide exactly with those given by KT in the limit $Re\to\infty$ (and previous works on the inviscid stability of Long's vortex; see the next section for the specific relations between the notation in KT and that used here). However, for $\Delta\neq0$ (viscous problem), in addition to the fact that here $m\neq1$, some new terms proportional to $\Delta$ appear in (3.7)–(3.10) which are missing in the equivalent equations by KT for $m=1$. These new terms come from the axial derivatives of both the mean flow and the amplitude of the perturbations, non-parallel effects which were neglected in KT and most previous works. But the changes in the $z$-direction of the flow give rise to terms in the equations of the same order as the viscous terms, i.e. they are linear in $\Delta$, and must consequently be retained. In other words, for the family of vortices analysed here, which includes Long's vortex as the case $m=1$, the parallel-flow approximation is only consistent in the inviscid limit of the stability analysis. It should be mentioned here that non-parallel effects were considered by Foster & Jacqmin (1992) in the instability of Long's vortex. These authors considered, however, only Type II vortices in the asymptotic limit of large flow force $M$ ($m=1$ and $A_1\to-1/\sqrt{2}$ in the present notation).

Equations (3.7)–(3.10) constitute a linear system of ordinary differential equations for the $\xi$-dependence of the amplitude of the perturbations, which, together with the boundary conditions (3.11)–(3.14), form an eigenvalue problem for the frequency $\omega$ (see below). It should be noted that the axial coordinate $z$ enters into (3.7)–(3.10) as a parameter (through $\Delta$, and embedded in $\xi$, $\omega$ and $\alpha$). That is, non-parallel effects are taken into account locally, by considering the rate of axial change of both the mean flow and the amplitude of the perturbations, which give rise to terms as important as the viscous ones. Thus, the temporal stability or instability of the mean flow is implicitly a function of $z$. The approximation assumes that the axial characteristic length of the basic flow is large compared to the perturbation wavelength. Therefore, the results given below have to be cautiously considered when $\alpha$ is very small. In that case, the axial variation of the mean flow has to be taken into account globally: one has to integrate the evolution of the perturbations along the axial direction. The governing equations become then a system of partial differential equations instead of the ordinary differential equations (3.7)–(3.10).

To solve numerically (3.7)–(3.10), a staggered Chebyshev spectral collocation technique developed by Khorrami (1991*b*) is used. This method has the advantage of

eliminating the need for two artificial pressure boundary conditions at the domain end points $\xi = 0$ and $\xi = \infty$, which for that reason are not included in (3.11)–(3.14). The boundary conditions at infinity (3.11) are applied at a truncated radial distance $\eta_{max}$, chosen large enough to ensure that the results do not depend on that truncated distance. The computations showed that $\eta_{max} = 30$ ($\xi_{max} = 900$) was sufficient for most profiles to obtain an accuracy of six significant figures. Since the value of $\eta_{max}$ does not affect much the computation time, $\eta_{max} = 50$ ($\xi_{max} = 2500$) was used for all the reported computations. To implement the spectral numerical method, (3.7)–(3.10) are discretized by expanding the perturbation eigenfunctions in terms of truncated Chebyshev series. A non-uniform coordinate transformation is used to map the interval $0 \leqslant \xi \leqslant \xi_{max}$ into the Chebishev polynomials domain $-1 \leqslant s \leqslant 1$, $\xi = a(1+s)/(b-s)$, where $a$ is a constant ($a = 3$ in all the computations) and $b = 1 + 2a/\xi_{max}$ (Khorrami 1991*b*). This transformation allows large values of $\xi$ to be taken into account with relatively few basis functions. Equations (3.7)–(3.10) together with (3.11)–(3.14) are thus reduced to a generalized eigenvalue problem of the form

$$\boldsymbol{D}\boldsymbol{X} = \omega \boldsymbol{L}\boldsymbol{X}, \tag{3.15}$$

where $\boldsymbol{X}$ is the eigenfunction vector

$$\boldsymbol{X} = [FGH\Pi]^T, \tag{3.16}$$

and $\boldsymbol{D}$ and $\boldsymbol{L}$ are $4N \times 4N$ matrices, $N$ being the number of Chebyshev polynomials (see Khorrami 1991*b* for the details). The eigenvalue equation (3.15) is solved here by using the IMSL subroutine DGVLCG (and DGVCCG), which provides the entire eigenvalue spectrum (and the eigenvectors). $N$ was varied in the range $40 \leqslant N \leqslant 100$, so that an accuracy of at least six significant figures was attained (as discussed by Mayer & Powell 1992, the closer to neutral stability of a given unstable mode, the higher the accuracy needed to reveal it).

## 4. The stability of Long's vortex

This section considers the case $m = 1$ or Long's vortex. First, in order to test the numerical method and check the accuracy of the results, a comparison is made with the results given by KT (it must be noted here that KT corrected and extended previous results by Foster & Duck 1982 on the inviscid stability of Long's vortex; see below). To that end the profile named by KT as Long-I is chosen, which corresponds to the Type I solution for $M = 4.0$ ($A_1 \simeq 0.42, A_2 \simeq 0.60$, and $B \simeq 2.36$ in (2.11) and (2.12); see figure 3*a* for the velocity profiles). To make possible the comparison, the following relations between the notation of KT and the present one are used (note that $m = 1$):

$$\alpha_{KT} = \frac{\sqrt{2}}{B}\alpha, \quad \omega_{KT} = \frac{2}{B^3}\omega, \quad Re_{KT} = \frac{B}{\Delta}. \tag{4.1}$$

The dimensionless radial distance of KT is related to $\eta$ through $r_{KT} = B\eta/\sqrt{2}$. Thus, $\eta_{max} = 50$ corresponds to a maximum value of $r_{KT}$ approximately equal to 83 for the profile under consideration, which is beyond the maximum used by KT.

Figure 3(*b*) displays the same curves as figures 4 and 6 of KT; namely, the variation of the growth rate $\omega_i$ for the most unstable mode with Reynolds number for some values of $n \neq 0$ and $\alpha$. It is observed that the asymptotes for high Reynolds numbers of the different cases represented coincide exactly with those obtained by KT. Since for $\Delta = 0$ and $m = 1$ both sets of equations are identical, this agreement

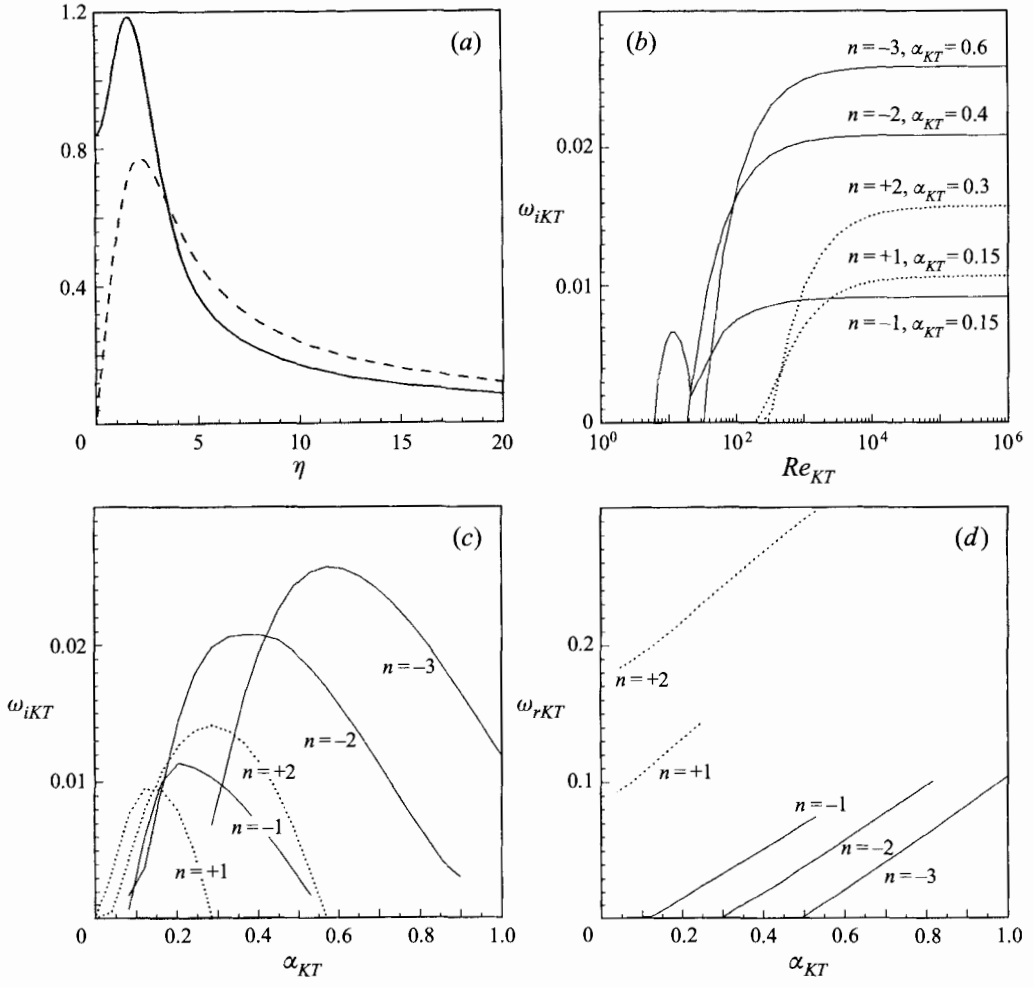


FIGURE 3. Results for Long-I profile of KT ($m = 1$). (*a*) Axial (continuous line) and azimuthal (dashed line) velocity profiles (Long-I corresponds to Type I solution for $M = 4$ or $A_1 = 0.42$ in figure 2*a*). (*b*) Maximum growth rate as a function of the Reynolds number for some asymmetric modes ($n \neq 0$) with different axial wavenumbers. KT notation is used (see (4.1)). (*c,d*) Maximum growth rate and real part of the frequency as a function of the axial wavenumber for the case given in (*b*) when $Re_{KT} = 4000$.

constitutes a favourable test of the numerical method and its accuracy. For moderate Reynolds numbers ($\Delta \neq 0$, but small), some additional terms appear in (3.7)–(3.10) in relation to the equivalent equations by KT, as discussed above. However, the obtained values of $\omega_i$, and even the critical Reynolds numbers for the different modes, practically coincide with those reported by KT, except for $n = -1$. For this azimuthal wavenumber it is found that a higher mode becomes more unstable than the main inviscid one when $Re_{KT}$ approaches the value corresponding to the neutral stability of the most unstable inviscid mode. Thus, a purely viscous unstable mode, similar to those reported by Khorrami (1991*a*) in relation to the trailing line vortex, appears here for Long's vortex. This viscous mode was not found by KT. Indeed, these authors did not find any purely viscous unstable mode for Long's vortex after "an extensive search". Hence, the unstable viscous mode for $n = -1$

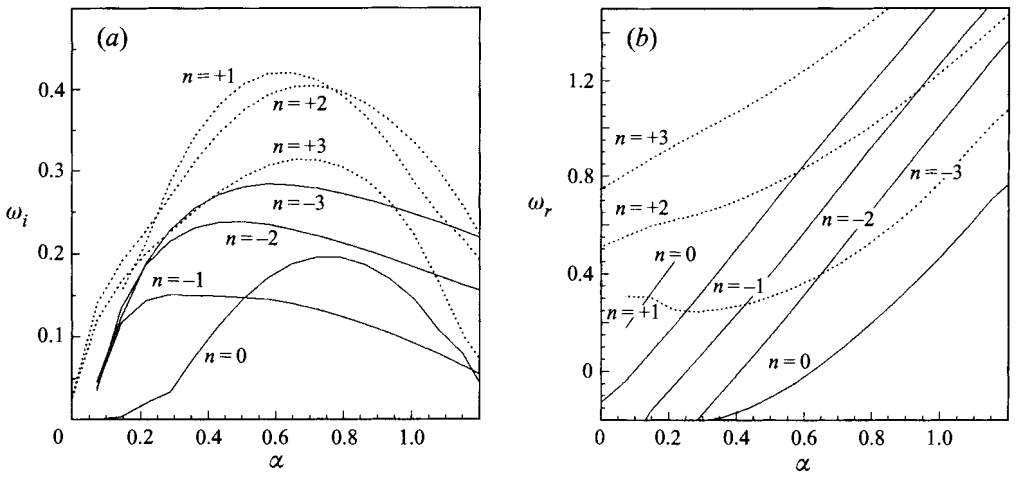


FIGURE 4. Maximum growth rate (*a*) and real part of the frequency (*b*) as a function of the axial wavenumber for $m = 1$, $A_1 = -0.6$ (Type II solution with $M = 7.09$) and $\Delta = 0$, for several values of the azimuthal wavenumber $n$.

of figure 3(*b*) is presumably due to the non-parallel effects, neglected by KT. This phenomenon of mode crossing and switching for disturbances with $n = -1$ is not new. It was reported by Khorrami (1992) in relation to the instability of a trailing line vortex, and, earlier, by Cotton & Salwen (1981) for rotating Hagen–Poiseuille flows.

To complete the comparison with the results given by KT for the Long-I vortex, figures 3(*c*) and 3(*d*) display the variation of the imaginary and real and parts of the frequency with the axial wavenumber for the same cases as in figures 3 and 5 of KT. As expected from the very small value of $\Delta$ ($\Delta = 0.00059$, corresponding to $Re_{KT} = 4000$ for the Long-I vortex), the agreement between both sets of figures is very good.

In addition to the purely viscous unstable mode for $n = -1$ just reported, we have found others for different values of $n$, $\alpha$ and $A_1$. More relevant is, perhaps, the fact that we have also found inviscid unstable modes for axisymmetric disturbances ($n = 0$). Neither of these were uncovered by KT. Therefore, it seems of interest to provide a more detailed map of instability for Long's vortex, which is given next.

### 4.1. *Inviscid instabilities*

The variation of the frequency with the axial wavenumber for three representative vortices ($A_1 = -0.6$, corresponding to a Type II solution; $A_1 = 1.2$, a Type I solution, and $A_1 = 0.15$, approximately the critical or folding value; see figure 2), and azimuthal wavenumbers $n = 0, \pm 1, \pm 2, \pm 3$, is displayed in figures 4–6 for the most unstable modes with $\Delta = 0$.

According to figure 4(*a*), the velocity profile for $A_1 = -0.6$, which corresponds to a two-cell vortex with negative axial velocity at the axis and a marked maximum outside it (see figure 2*b*), is unstable for all seven azimuthal wavenumbers represented, including axisymmetric disturbances ($n = 0$), in a wide range of the axial wavenumber. The growth rate is larger for $n > 0$ disturbances than for $n \leqslant 0$ ones. For $n = 0$, the maximum growth rates represented in figure 4(*a*) correspond to two different modes as $\alpha$ increases, as it is more evident in figure 4(*b*), where the real part of the corresponding frequency presents a discontinuity for the values of $\alpha$ where the curve

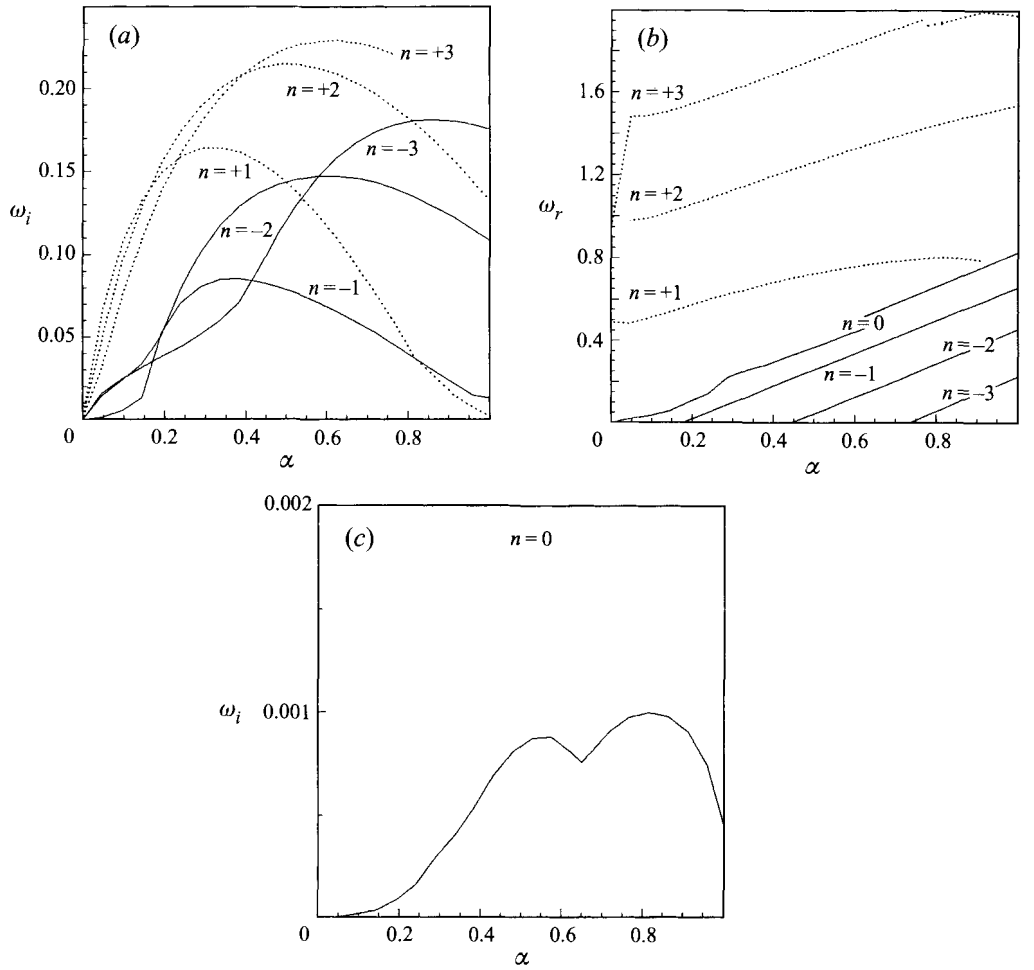


FIGURE 5. Maximum growth rate (*a*) and real part of the frequency (*b*) as a function of the axial wavenumber for $m = 1$, $A_1 = 0.15$ (folding value, $M = 3.75$), and $\Delta = 0$, for several values of $n \neq 0$. (*c*) Growth rate for axisymmetric disturbances ($n = 0$).

$\omega_i(\alpha)$ changes its slope. Figure 4(*b*) also shows that the real part of the frequency for $n \leqslant 0$ has a linear variation with $\alpha$, with approximately the same slope for all the modes (for $n = 0$ this is so before the mode switching). For $n > 0$ (and for $n = 0$ after the mode switching), $\omega_r(\alpha)$ is no longer a simple linear relation. These general features of $\omega_r(\alpha)$ are also observed for the other two profiles represented (figures 5*b* and 6*b*), and are in agreement with KT. The slopes for the negative azimuthal wavenumbers depends on $A_1$.

The main difference between the stability characteristics for the case $A_1 = -0.6$ just described and the profile for $A_1 = 0.15$ (corresponding to the folding value of $L(A_1)$, and representing a single-cell vortex, with no region of axial flow reversal, but with the maximum of the axial velocity outside the axis; see figure 2) is that the unstable axisymmetric mode has almost disappeared, having a maximum growth rate two orders of magnitude smaller than for $n \neq 0$ (figures 5*a* and 5*c*). Also, the peak growth rates for the $n \neq 0$ modes are about half of the corresponding ones for the profile with $A_1 = -0.6$.

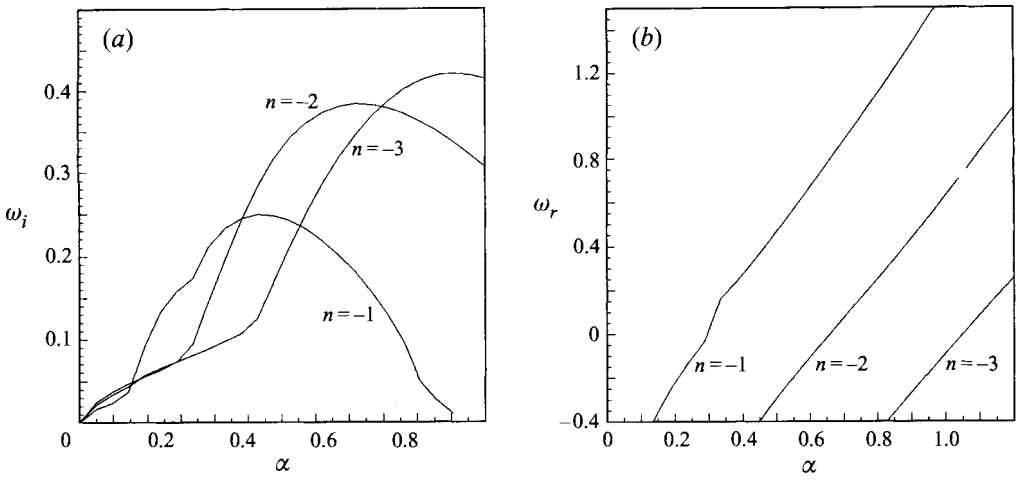


FIGURE 6. Maximum growth rate (*a*) and real part of the frequency (*b*) as a function of the axial wavenumber for $m = 1$, $A_1 = 1.2$ (Type I solution with $M = 6.838$) and $\Delta = 0$, for several values of $n$.

For the velocity profile with $A_1 = 1.2$, representing a single-cell jet-like vortex, with a marked maximum axial velocity at the axis, no unstable modes with $n \geqslant 0$ are found (figure 6*a*).

In view of the important variations in the stability characteristics as the parameter $A_1$ changes, it is interesting to map the growth rate for the different azimuthal modes in the $(\alpha, A_1)$-plane. To that end, this plane was discretized for $0 \leqslant \alpha \leqslant 1.8$ and $-0.7 \leqslant A_1 \leqslant 1$, and the stability equations solved numerically at each point. Figure 7 displays the contours of constant growth rate in the $(A_1, \alpha)$-plane for axisymmetric disturbances, $n = 0$, and two representative non-axisymmetric disturbances, $n = \pm 1$. (All the results given in this work which are presented in the form of a topographical map on the $(\alpha, A_1)$-plane are computed using $N = 100$.) The largest unstable region corresponds to $n = -1$ (figure 7*b*), for which all the profiles depicted ($-0.6 \leqslant A_1 \leqslant 1$) are unstable in some interval of the axial wavenumber. The smallest peak growth rate for $n = -1$ occurs at $A_1 \simeq 0.8$, and grows as $A_1$ goes to its extreme values, $-1/\sqrt{2}$ and infinity. For all values of $A_1$ shown, the peak growth rates correspond to $\alpha$ slightly smaller than 0.4. In the case of disturbances with $n = 1$ (figure 7*a*), although the peak growth rates are significantly larger than for $n = -1$ when $A_1 < 0$, no unstable modes are found for $A_1 > 0.6$, approximately. Finally, unstable axisymmetric ($n = 0$) modes are only found for $A_1$ smaller than approximately 0.2 (figure 7*c*). Thus, Type I vortices are stable for axisymmetric disturbances. Except for the interval $0.15 < A_1 < 0.6$, approximately, they are also stable for disturbances with positive azimuthal wavenumbers. On the other hand, Type II vortices are found unstable for disturbances with any value of the azimuthal wavenumber in some range of the axial wavenumber. In fact, as shown in figure 8, $\omega_i$ grows very fast as $A_1 \to -1/\sqrt{2}$ for $\alpha = O(1)$. This figure shows the $\alpha = 0.432$ cross-section of the three surfaces $\omega_i(\alpha, A_1)$ depicted topographically in figure 7 (the results for $A_1 < -0.6$ are not shown in figure 7 to avoid cluttering).

The inviscid instability features for Long's vortex just described agree with the asymptotic results by Foster & Smith (1989) and by Ardalan *et al.* (1995). Most of them also coincide with the more complete results given by KT. For instance, these

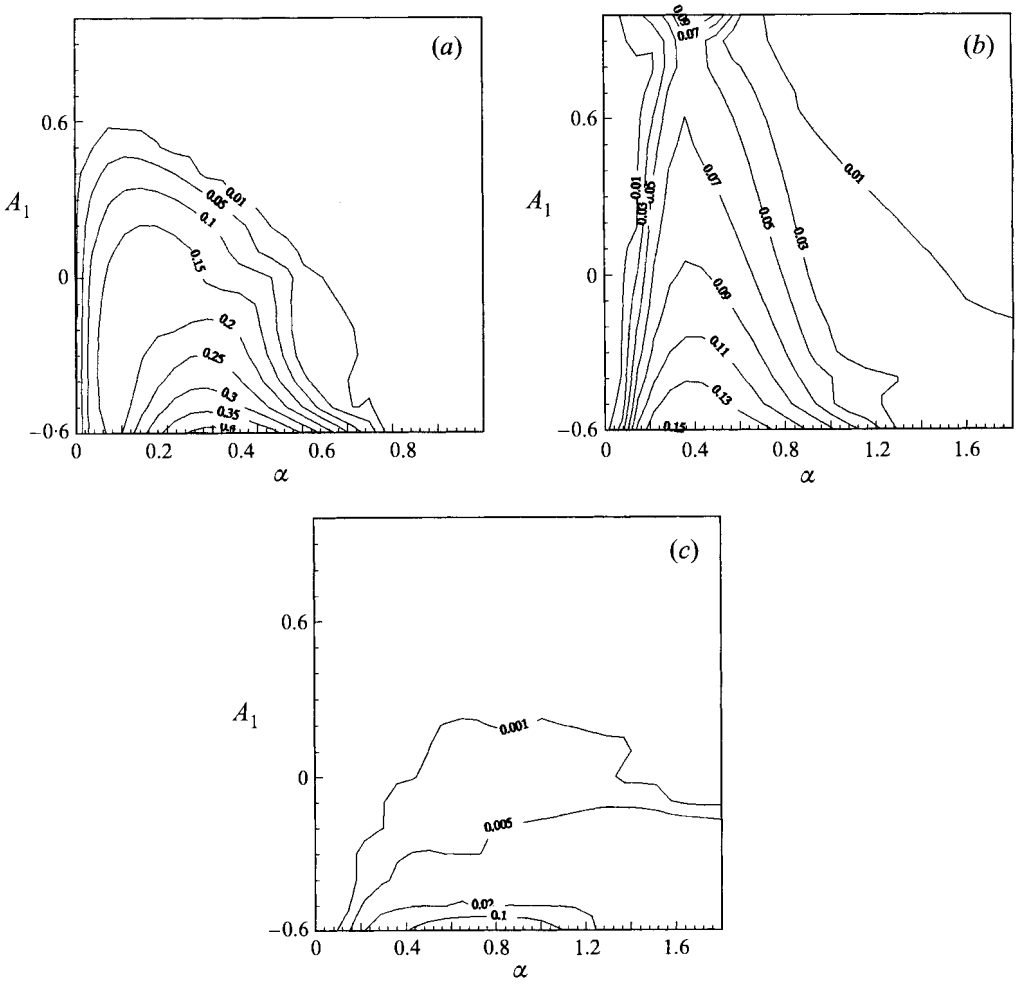


FIGURE 7. Contours of constant growth rate for the most unstable inviscid ($\Delta = 0$) mode in the $(\alpha, A_1)$-plane for $m = 1$ and $n = 1$ (*a*), $n = -1$ (*b*), and $n = 0$ (*c*).

last authors found that their Long-III vortex, corresponding to $A_1 \simeq 0.8$, is unstable only for disturbances with $n < 0$, while the other three profiles (Long-I, $A_1 \simeq 0.42$; Long-II, $A_1 \simeq -0.15$, and Long-IV, $A_1 \simeq -0.4$) are unstable for both $n < 0$ and $n > 0$ modes, in agreement with the present results. It should be noted here that these last inviscid unstable modes with positive azimuthal wavenumber were not found in the earlier work by Foster & Duck (1982) on the inviscid stability of Long's vortex. KT showed that this was due to the truncation made by those authors of the infinite radial domain into a small computation domain (these positive-$n$ modes were nonetheless found later by Foster & Smith 1989 in their asymptotic analysis of Type II vortices in the limit of large values of $M$). However, as an important difference with the present inviscid results, KT did not find any axisymmetric ($n = 0$) unstable mode. This was so even for their Long-IV vortex, which presents a marked two-cell structure and, according to figures 7 and 8, the growth rate for axisymmetric disturbance is only about one order of magnitude smaller than for the non-axisymmetric ones (for their Long-II vortex it is also found here that the axisymmetric disturbances are unstable, but in this case the growth rate is two orders of magnitude smaller than

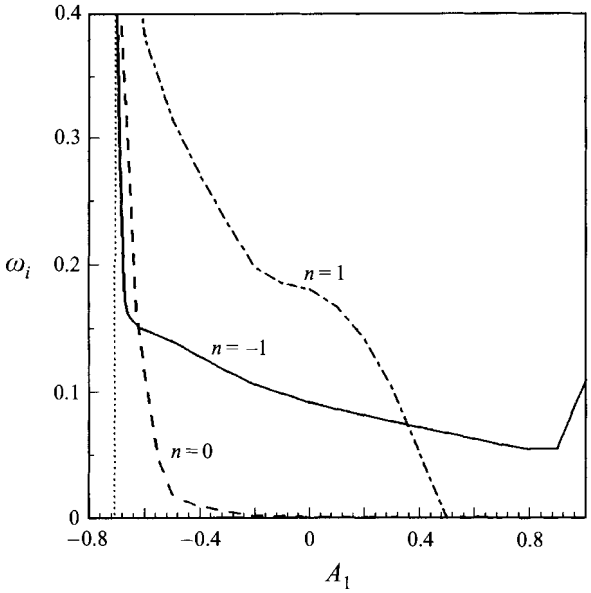


FIGURE 8. Maximum growth rate as a function of $A_1$ for $\alpha = 0.432$ and the same values of $m$, $\Delta$ and $n$ as figure 7. Several mode switchings occur, characterized by a change in the curvature or by an abrupt change of slope.

the growth rate for the non-axisymmetric disturbances). For the inviscid instabilities considered in this section this disagreement seems surprising since the non-parallel effects are null and, consequently, KT's linear stability equations coincide exactly with those used here for $m = 1$. The explanation may lie in that most of the results given by KT are for $Re_{KT} = 10^4$, which for the Long-IV vortex corresponds to $\Delta \simeq 8.6 \times 10^{-4}$. It is shown below (see figure 14) that the neutral curve in the $(\alpha, A_1)$-plane for axisymmetric disturbances and $\Delta = 0.001$ lies, for moderate values of $\alpha$, at $A_1 \simeq -0.4$, which corresponds to the Long-IV vortex of KT. Thus, the Long-IV vortex is stable for axisymmetric disturbances when $Re_{KT} = 4000$. In addition, KT did not present detailed results for the Long-IV vortex, just stating that "preliminary analysis of the Long-IV vortex revealed stability characteristics resembling that of the Long-II vortex", so that "the analysis and discussion of Long-IV is omitted here". But it is shown here that, though the growth rate for the axisymmetric disturbances of Long-II is very small, this is not so for Long-IV. Indeed, figure 8 shows that for velocity profiles with marked two-cell features ($A_1 < -0.6$, approximately), the growth rates for axisymmetric and non-axisymmetric disturbances are of the same order. Thus, Type II Long vortices with large values of $M$ ($A_1 \to -1/\sqrt{2}$) are found unstable, with comparable growth rate, for all – positive, negative, and null azimuthal wavenumbers $n$. This is in agreement with the asymptotic results by Foster & Smith (1989). In the opposite limit of Type I vortices with large $M$ ($A_1$ large), only the perturbations with negative values of the azimuthal wavenumber are here found unstable. For $A_1 > 0.9$, approximately, it is found that the growth rate for constant $\alpha$ increases linearly with $A_1$ (see figure 8 for $n = -1$), in agreement with the asymptotic results by Ardalan *et al.* (1995) in this limit (note in figure 2 that $M$ increases linearly with $A_1$ for $A_1 > 0.8$, approximately).

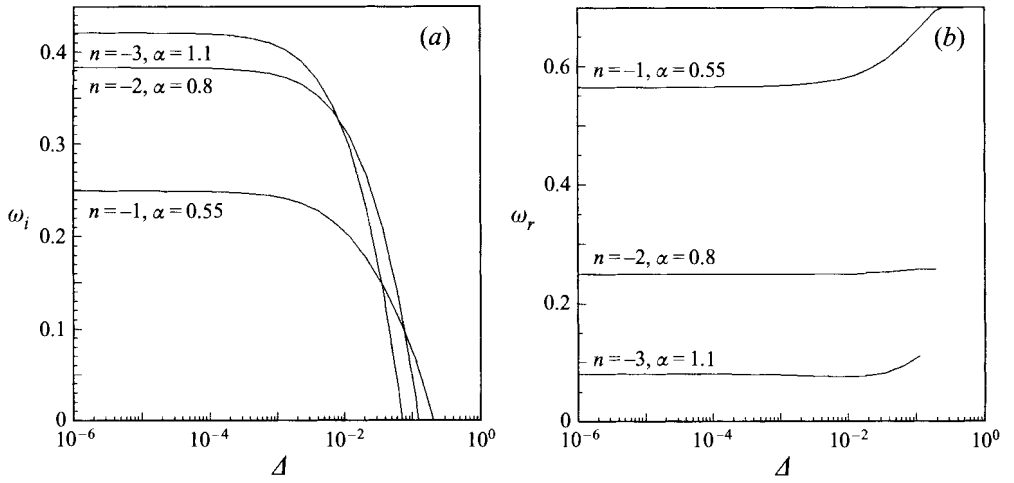


FIGURE 9. Maximum growth rate (*a*) and real part of the frequency (*b*) as a function of $\Delta = Re^{-1}$ for $m = 1$, $A_1 = 1.2$ (Type I solution with $M = 6.838$), and the values of $\alpha$ and $n$ corresponding to the peak growth rates of figure 6.

### 4.2. *Effects of viscosity on inviscid modes and viscous instabilities*

Figures 9–11 show the effect of viscosity on the frequency of the most unstable inviscid modes for values of $\alpha$ and $n$ corresponding to the peak growth rates represented in figures 4–6. For a typical Type I vortex (see figure 9 for $A_1 = 1.2$), the critical values of $\Delta$, $\Delta_c$, for the unstable modes with $n < 0$ are very close and $O(10^{-1})$ (the critical Reynolds numbers, $Re_c$, are $O(10)$). For $\Delta < \Delta_c$ ($Re > Re_c$) the growth rates increase very rapidly until they reach their inviscid values when $\Delta = O(10^{-3})$. The real part of the frequencies (figure 9*b*) decrease smoothly for $\Delta < \Delta_c$, approaching their inviscid values even faster than the corresponding growth rates. This is common to all the cases considered, so that no more figures for $\omega_r(\Delta)$ are given.

Near the folding value of $M$ (figure 10 for $A_1 = 0.15$) the vortex is also unstable for disturbances with $n \geqslant 0$. For $n < 0$, $\Delta_c$ is again $O(10^{-1})$, while for $n > 0$ $\Delta_c$ is slightly smaller (the critical Reynolds number is larger), which is in agreement with the results given by KT for the Long-I vortex (see figure 3*b*). For $n = 0$ disturbances, for which the peak inviscid growth rates are about two orders of magnitude smaller than for $n \neq 0$, $\Delta_c$ is considerably smaller, between $10^{-6}$ and $10^{-5}$ (figure 10*b*). Thus, the axisymmetric unstable modes for Long's vortex become stabilized by viscosity at Reynolds numbers much larger than the non-axisymmetric ones ($Re_c = O(10^5)$).

An important difference with the Type I vortex is the appearance of a purely viscous unstable mode for $n = -1$ (figure 10*a*), similar to that depicted in figure 3*b* for $A_1 = 0.42$. Although it was known for quite a long time that viscosity, in addition to the stabilizing effect, can also destabilize some flows, no evidence of viscous instabilities for swirling flows was found until the work by Khorrami (1991*a*) on the viscous stability of a trailing (Batchelor's) vortex. However, more recently, KT found no viscous unstable modes for the Long's vortex considered here, so that, to our knowledge, this is the first evidence of them. The viscous mode for $n = -1$ depicted in figure 10(*a*) has a peak growth rate about one order of magnitude smaller than the most unstable inviscid mode for the same value of $n$, and it occurs at a value of $\Delta$ slightly larger than the critical value for that inviscid mode ($\Delta = O(10^{-1})$). These characteristics are in qualitative agreement with those found for the viscous unstable

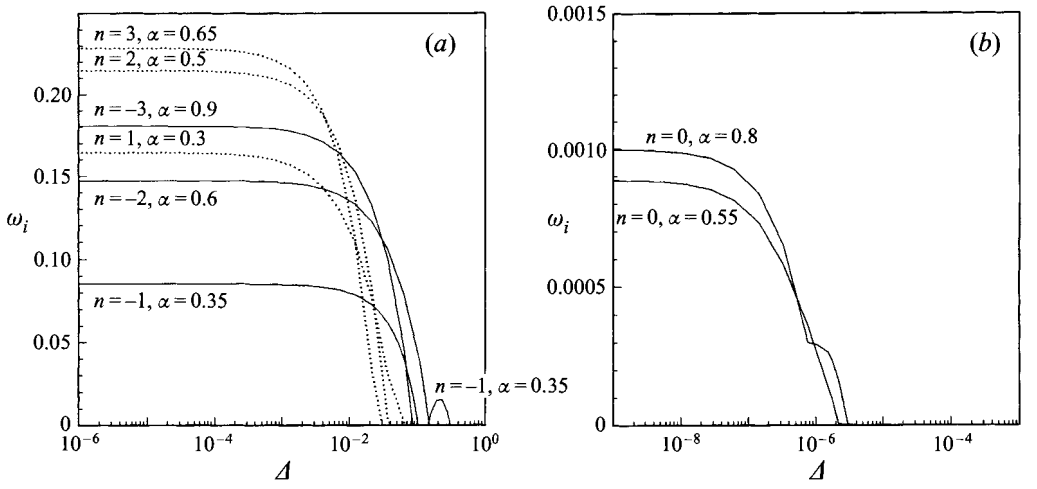


FIGURE 10. Maximum growth rate as a function of $\Delta = Re^{-1}$ for $m = 1$, $A_1 = 0.15$ (folding value), and the values of $\alpha$ and $n$ corresponding to the peak growth rates of figure 5. (*a*) $n \neq 0$. (*b*) $n = 0$.

modes of Batchelor's vortex (Khorrami 1991*a*; Mayer & Powell 1992). For $n = 0$ and $\alpha = 0.8$ (figure 10*b*), a second mode becomes more unstable than the most unstable inviscid one near $\Delta_c$. In fact, although not shown in the figures, there are higher unstable modes associated with the given values of $n$ and $\alpha$ which always have lower growth rates than the primary modes.

For the Type II vortex considered ($A_1 = -0.6$; figure 11), viscous unstable modes appear for all the values of $n$ represented when $\Delta = O(10^{-1})$. In fact, for some values of $n$, two or more viscous unstable modes appear, as is shown more clearly for $n = -1$. The number of viscous modes increases as $\Delta$ approaches unity, but for such low Reynolds numbers the boundary layer approximation of this work is no longer valid, and these results are not given in figure 11.

The fact that viscous unstable modes appear for some velocity profiles makes it of interest to map the maximum growth rate in the $(A_1, \alpha)$-plane for different values of $n$ as $\Delta$ increases (Reynolds number decreases). This will also show more precisely how viscosity affects the inviscid modes, and the main differences between viscous and inviscid unstable modes. Figures 12–14 show the contours of constant growth rate in the $(A_1, \alpha)$-plane for $n = -1$, $n = 1$, and $n = 0$, respectively, and for increasing values of $\Delta$. When $\Delta = 10^{-3}$, the contour lines for $\omega_i \geqslant 0.02$ approximately, practically coincide with the inviscid ones (figure 7). Obviously, this is in agreement with the results just described for the effect of viscosity on the peak growth rates of the inviscid unstable modes. However, for very small growth rates, the inviscid unstable regions in the $(A_1, \alpha)$-plane are larger than for $\Delta = 10^{-3}$, especially for axisymmetric disturbances. As also shown above, the inviscid unstable modes with $n = 0$ for $A_1 = 0.15$, which as seen in figure 14(*a*) do not exist even for $\Delta = 10^{-4}$, have very small growth rates. Figure 10(*b*) shows that the growth rate for $A_1 = 0.15$ becomes positive for $\Delta$ below $10^{-5}$, so that axisymmetric instabilities for $A_1 = 0.15$ show up at Reynolds numbers larger than those represented in figure 14. In any case, axisymmetric instabilities appear only for Type II vortices ($A_1 < 0.2$, approximately). The comparison of figures 12(*a*) and 13(*a*) with figures 7(*a*) and 7(*b*) shows that these unstable inviscid modes with very small growth rates also appear for non-

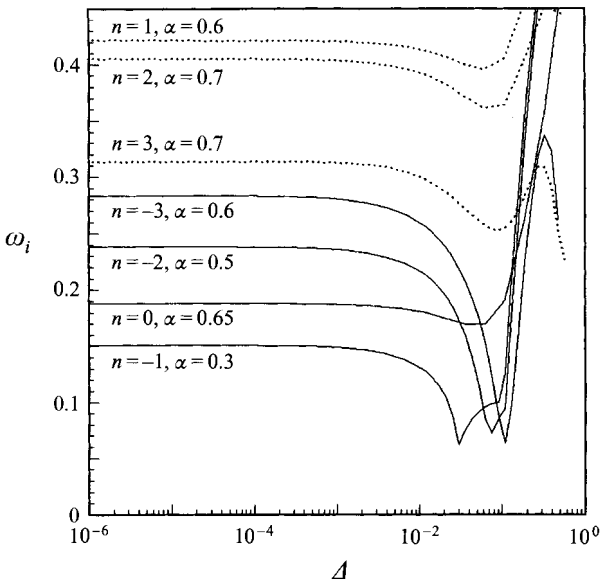


FIGURE 11. Maximum growth rate as a function of $\Delta = Re^{-1}$ for $m = 1$, $A_1 = -0.6$ (Type II solution with $M = 7.09$), and the values of $\alpha$ and $n$ corresponding to the peak growth rates of figure 4.

axisymmetric disturbances in Type II vortices for relatively large values of $\alpha$ (i.e. small-wavelength disturbances).

Two important features are observed in figure 12 for $n = -1$ disturbances as $\Delta$ increases above $10^{-2}$ ($Re$ decreases below 100). First, there is a shift of the peak growth rates of the inviscid unstable modes to smaller axial wavenumbers, so that viscosity stabilizes faster shorter-wavelength disturbances. This viscosity damping of the inviscid modes is also faster for Type I than for Type II vortices. Secondly, viscous unstable modes appear, with peak growth rates significantly larger than the inviscid ones, for Type II vortices (in particular they are concentrated for $A_1 < -0.5$, approximately, increasing the peak growth rate very fast as $A_1 \to -1/\sqrt{2}$) and $\alpha$ of order unity. In this region of the $(A_1, \alpha)$-plane the inviscid unstable modes have practically vanished for $\Delta = 10^{-1}$.

For $n = 1$ disturbances (figure 13), no viscous unstable modes in exactly the above sense appear. But in a small region of the $(A_1, \alpha)$-plane, which practically coincides with that where the viscous unstable modes for $n = -1$ disturbances appear, there is no appreciable viscous stabilization of the inviscid unstable modes, the growth rate for $\Delta = 10^{-1}$ being almost the same as for $\Delta = 0$. Viscous damping of the inviscid unstable modes is thus much faster for Type I vortices and for large $\alpha$, being practically null in the small region of the parametric plane just mentioned. A similar situation occurs for axisymmetric disturbances (figure 14). The difference is that the viscous stabilization occurs at much higher Reynolds numbers and it affects unstable modes with much smaller growth rates. In addition, when $n = 0$ purely viscous unstable modes appear with rather small axial wavenumbers (large wavelengths). However, these last unstable modes with $\alpha \ll 1$ should be cautiously considered because of the local character of the non-parallel analysis performed here (see §3).

As mentioned above, non-parallel effects in the stability of Long's vortex have also been considered by Foster & Jacqmin (1992) in the limit of large $M$ for Type II

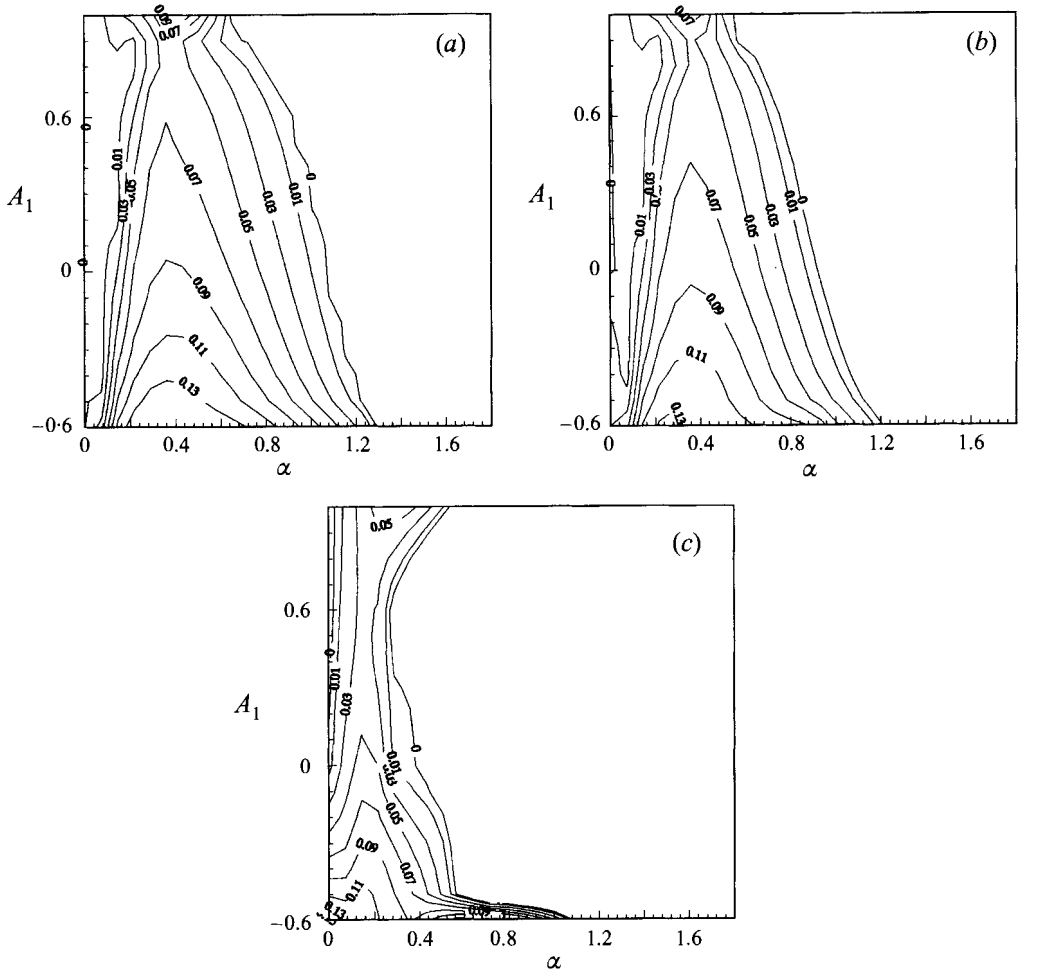


FIGURE 12. Contours of constant growth rate of the most unstable modes in the $(\alpha, A_1)$-plane for $m = 1$, $n = -1$, and three increasing values of $\Delta$: 0.001 (*a*), 0.01 (*b*), and 0.1 (*c*).

vortices ($A_1 \to -1/\sqrt{2}$). These authors thus extended the asymptotic results by Foster & Smith (1989) to account for effects of finite Reynolds number. They showed that in this large-$M$ limit non-parallel effects are even more important than the viscous terms in determining the finite-$Re$ behaviour. One of the main results found by Foster & Jacqmin is that viscosity tends to stabilize the $n > 1$ modes more effectively than the $n < -1$ ones. This is in agreement with the results shown in figure 10(*a*), according to which this result can also be extended to $n = 1$ and $n = -1$.

## 5. Results for $m > 1$

An exhaustive search for inviscid and viscous instabilities, similar to that reported above for $m = 1$, has been carried out for $m = 1.1$ and $m = 1.2$. These two values of $m$ (particularly $m = 1.1$) are of interest because it was shown in FFB that many real vortex cores may be approximately described by the present self-similar solutions with $m$ slightly larger than unity. Except for the important difference that now these stability results are governed by a swirl parameter ($L$), rather than by a flow force

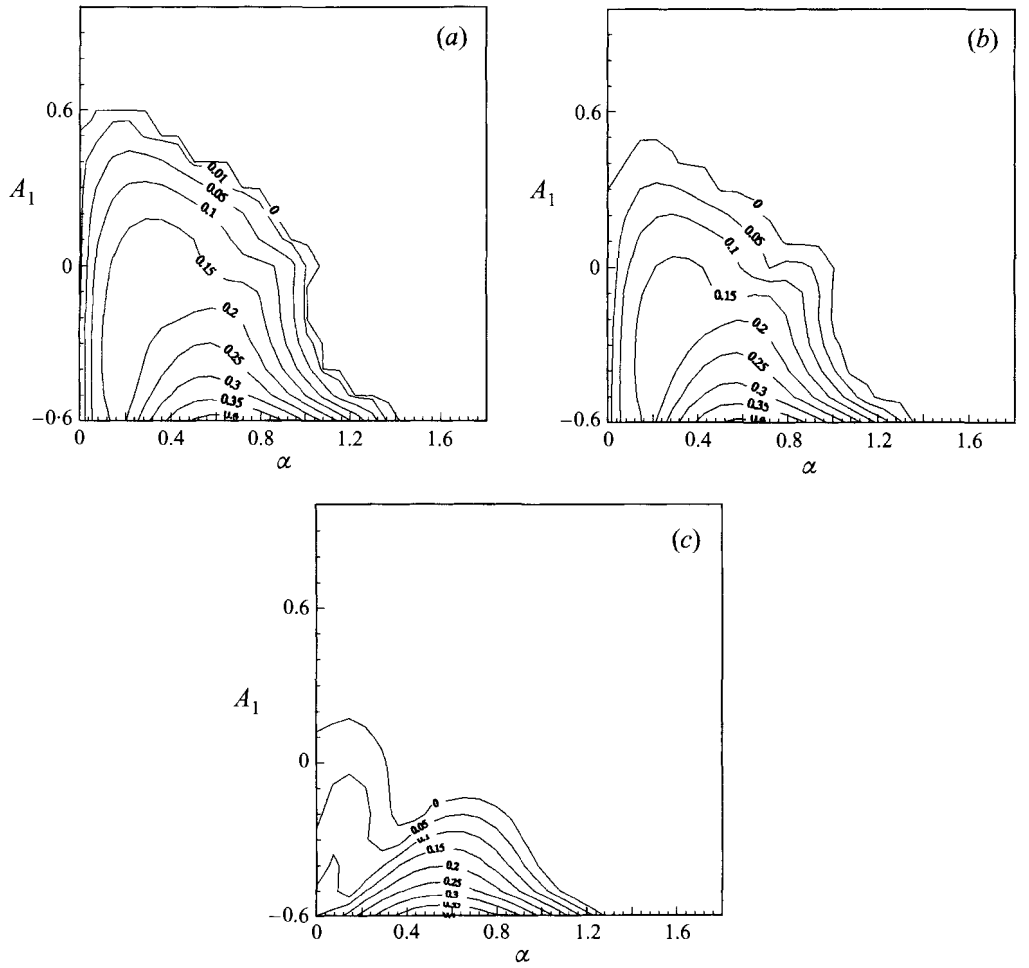


FIGURE 13. Contours of constant growth rate of the most unstable modes in the $(\alpha, A_1)$-plane for $m = 1$ and $n = 1$. $\Delta = 0.001$ (*a*), 0.01 (*b*), and 0.1 (*c*).

(*M*), as is the case in real vortex cores, the results are, in terms of $A_1$, very similar to those for $m = 1$ described above. Therefore, only the main, but relatively minor, distinctive features are reported here.

The differences are more significant for the inviscid unstable modes than for the viscous ones, and for $n \leqslant 0$ than for $n > 0$. As shown in figure 15, the map of the inviscid instabilities in the $(\alpha, A_1)$-plane for $n = 1$ disturbances are, for $m = 1.1$ and $m = 1.2$, almost identical with the corresponding one for $m = 1$ (figure 7*a*). For $n = -1$ (figure 16), the region of instabilities decreases as $m$ increases. The peak growth rate for Type II solutions (especially for $A_1 < -0.4$, approximately) increases and shifts to larger values of $\alpha$, while for Type I solutions it decreases and shifts to smaller values of $\alpha$ (larger wavelengths). The effect of increasing $m$ is thus somewhat analogous to the effect of viscosity when $n = -1$ (compare with figure 12). The most significant differences appear, however, for axisymmetric ($n = 0$) disturbances (figure 17). As $m$ increases, the peak growth rates for $A_1 < -0.4$ (approximately) increase, but the unstable region shrinks to smaller values of $A_1$. In particular, as a difference with $m = 1$, no unstable axisymmetric modes are found for the folding value

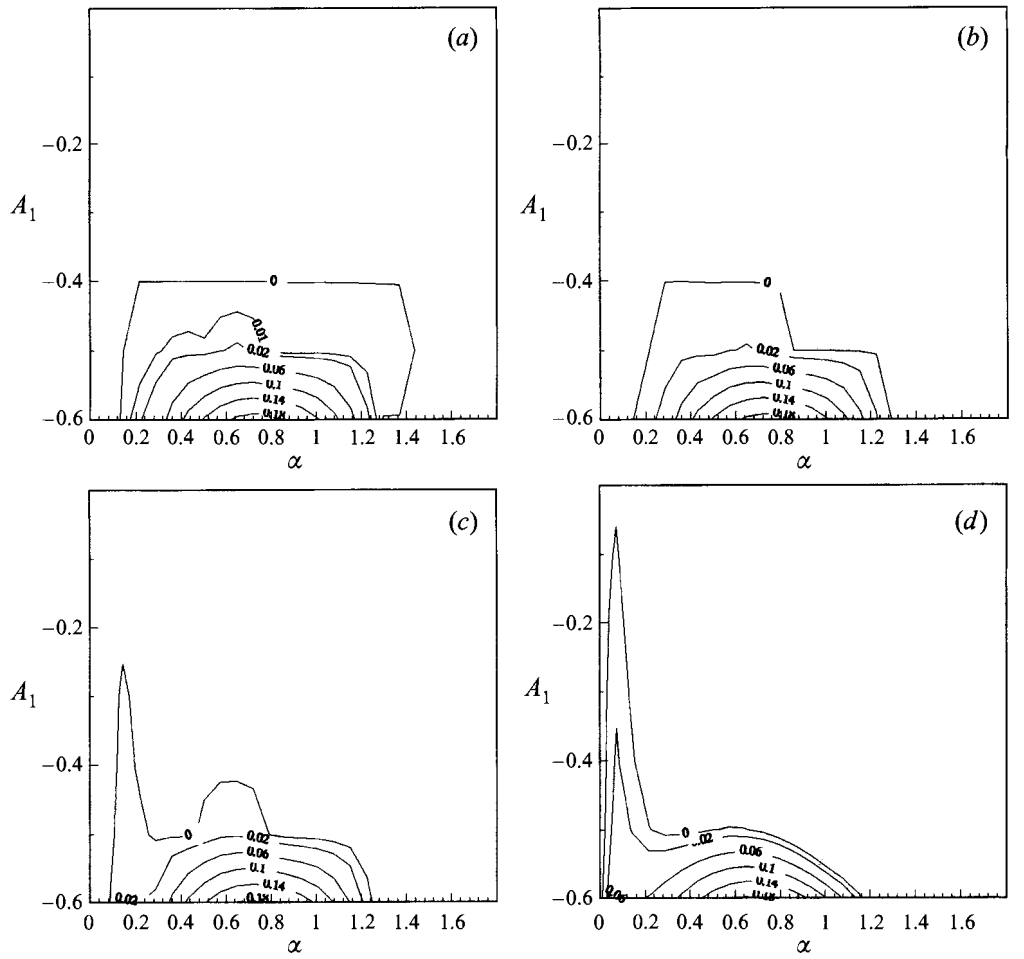


FIGURE 14. Contours of constant growth rate of the most unstable modes in the $(\alpha, A_1)$-plane for $m = 1$ and $n = 0$. $\Delta = 0.0001$ (*a*), 0.001 (*b*), = 0.01 (*c*), and 0.1 (*d*). Note the change in the scale of $A_1$ in relation to figures 12 and 13.

$A_1 \simeq 0.15$ when $m = 1.1$ (and, of course, when $m = 1.2$). Thus, the main distinction found between Type I and Type II solutions, the stability of Type I solutions under axisymmetric disturbances, is even sharper for $m > 1$ than for Long's vortex.

Regarding the viscous instabilities, the differences between Long's vortex and vortices with $m$ slightly larger than unity are even less important. Two distinctive features may be commented on. First, when $n < 0$, viscosity is more effective stabilizing inviscid modes for $m > 1$ than for $m = 1$ (see figure 18 for $m = 1.1$ and $n = -1$), except for purely viscous modes. Moreover, these last modes for $n = -1$ appear for smaller values of $A_1$ when $m > 1$. In particular, no unstable viscous mode appears for the folding value when $m > 1$. Thus, the other important distinction between Type I and Type II solutions, the presence of purely viscous unstable modes for Type II solutions, is again sharper for $m > 1$ than for $m = 1$.

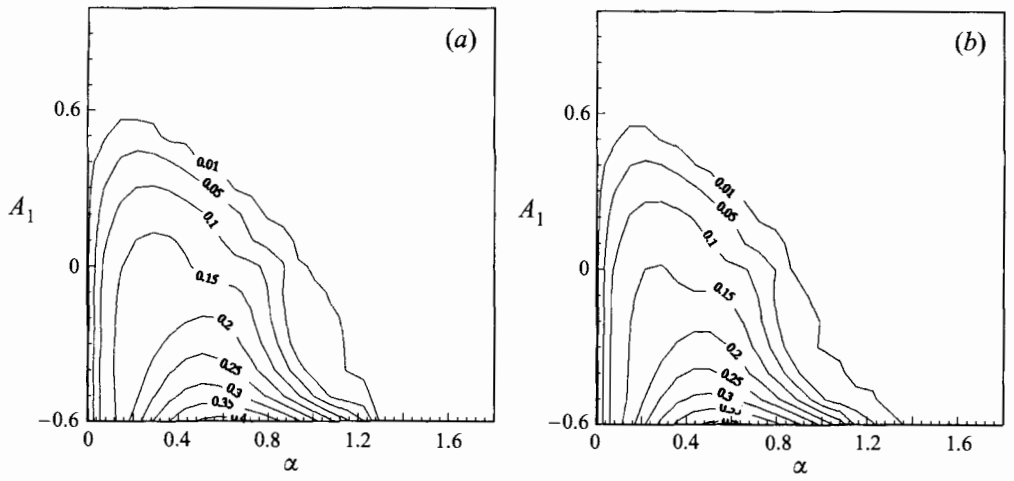


FIGURE 15. Contours of constant growth rate of the most unstable inviscid modes ($\Delta = 0$) in the $(\alpha, A_1)$-plane for $n = 1$, and for $m = 1.1$ (*a*) and $m = 1.2$ (*b*).

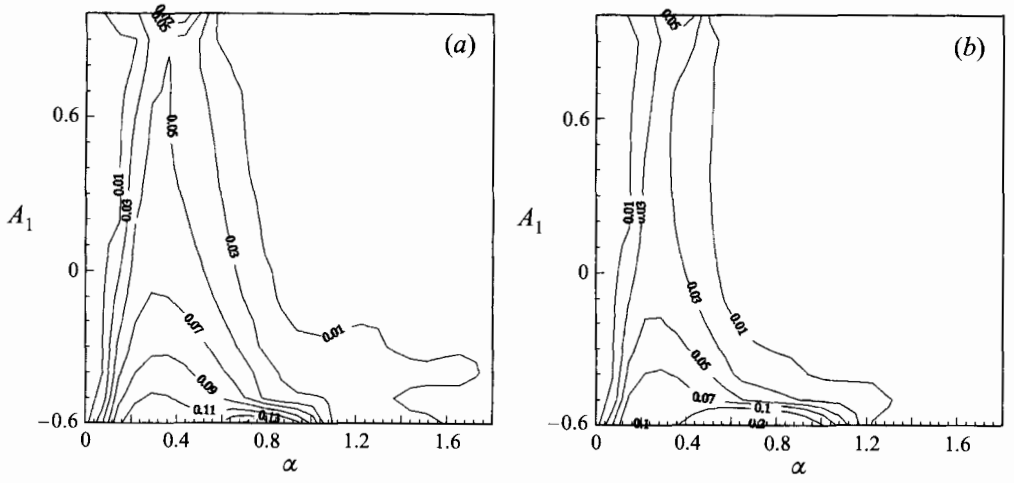


FIGURE 16. Contours of constant growth rate of the most unstable inviscid modes ($\Delta = 0$) in the $(\alpha, A_1)$-plane for $n = -1$, and for $m = 1.1$ (*a*) and $m = 1.2$ (*b*).

## 6. Summary and discussion

This paper has analysed the inviscid and viscous stability of a family of self-similar vortex cores. These flows correspond to exact solutions to the near-axis axisymmetric boundary layer equations matching external inviscid vortices with azimuthal velocity $V$ proportional to a negative power of the distance to the axis, $V \sim r^{m-2}$, with $0 < m < 2$. For $m = 1$ one has the well-known Long's vortex. However, experimental data show that the external inviscid azimuthal velocity surrounding many real vortex cores decreases with a power of $r$ corresponding to values of $m$ a little larger than unity (see e.g. Ogawa 1993). Particularly, the value $m \simeq 1.1$ is shown in FFB to best agree with experimental and numerical data for several confined and free vortex cores. The stability analysis has been performed for $m = 1$, $m = 1.1$ and $m = 1.2$. The results for the case $m = 1$ have been compared with previous ones on the stability of Long's vortex, especially with the recent work by KT, which extends and corrects previous

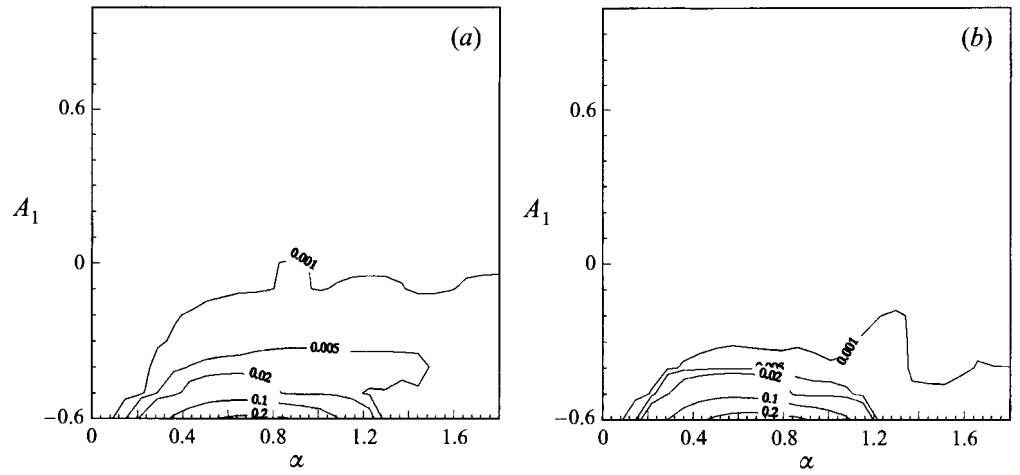


FIGURE 17. Contours of constant growth rate of the most unstable inviscid modes ($\Delta = 0$) in the $(\alpha, A_1)$-plane for $n = 0$, and for $m = 1.1$ (*a*) and $m = 1.2$ (*b*).

ones. As an important difference with most of these earlier works, non-parallel effects of the base flow have been retained in the linear equations for the perturbations. It is shown that these non-parallel effects enter these equations at the same level as the viscous terms, i.e. proportional to the inverse of the Reynolds number, which is assumed large (non-parallel effects were also considered in the instability of Long's vortex by Foster & Jacqmin 1992 in their asymptotic analysis for large values of $M$). Global pictures of the instabilities of Long's vortex are given here for the first time.

Although the results for $m = 1$ agree mostly with those given by KT on the stability of Long's vortex, new important unstable modes are found in this work which were not uncovered by KT. Of them, the most relevant are perhaps the inviscid unstable modes for axisymmetric disturbances ($n = 0$), found only for Type II solutions. This discrepancy in the results is not due to the non-parallel effects of the steady vortex because they do not affect to the inviscid modes. It is due, simply, to the fact that these authors did not analyse all the Long's solutions, but only four particular cases. Though two of them, Long-II and Long-IV, corresponding to $A_1 = -0.15$ and $A_1 = -0.4$, respectively, are found here to be unstable under inviscid axisymmetric perturbations, their corresponding growth rates are very small. Indeed, it is observed in figures 7(*c*) and 8 that, in spite of the fact that these axisymmetric disturbances become unstable for values of $A_1$ smaller than the critical or folding value ($A_1^* \simeq 0.15$), i.e. for Type II solutions, their growth rate becomes of the same order as the growth rate of the non-axisymmetric perturbations only for $A_1 < -0.6$, approximately. In addition, as observed in figure 14, for $A_1 > -0.4$, approximately, the inviscid unstable modes are stabilized by viscosity at relatively high Reynolds numbers (much higher than for non-axisymmetric disturbances), and all the results given by KT are for large but finite Reynolds numbers.

Purely viscous unstable modes for Long's vortex are also found in this work for the first time. That viscosity, in addition to its stabilizing effect on the inviscid unstable modes, may also have a destabilizing effect in swirling flows was first shown by Khorrami 1991*a* for the Batchelor's model of a trailing vortex. However the search by KT for these viscous unstable modes of Long's vortex was not successful. It seems therefore plausible that these viscous instabilities are due to the non-parallel

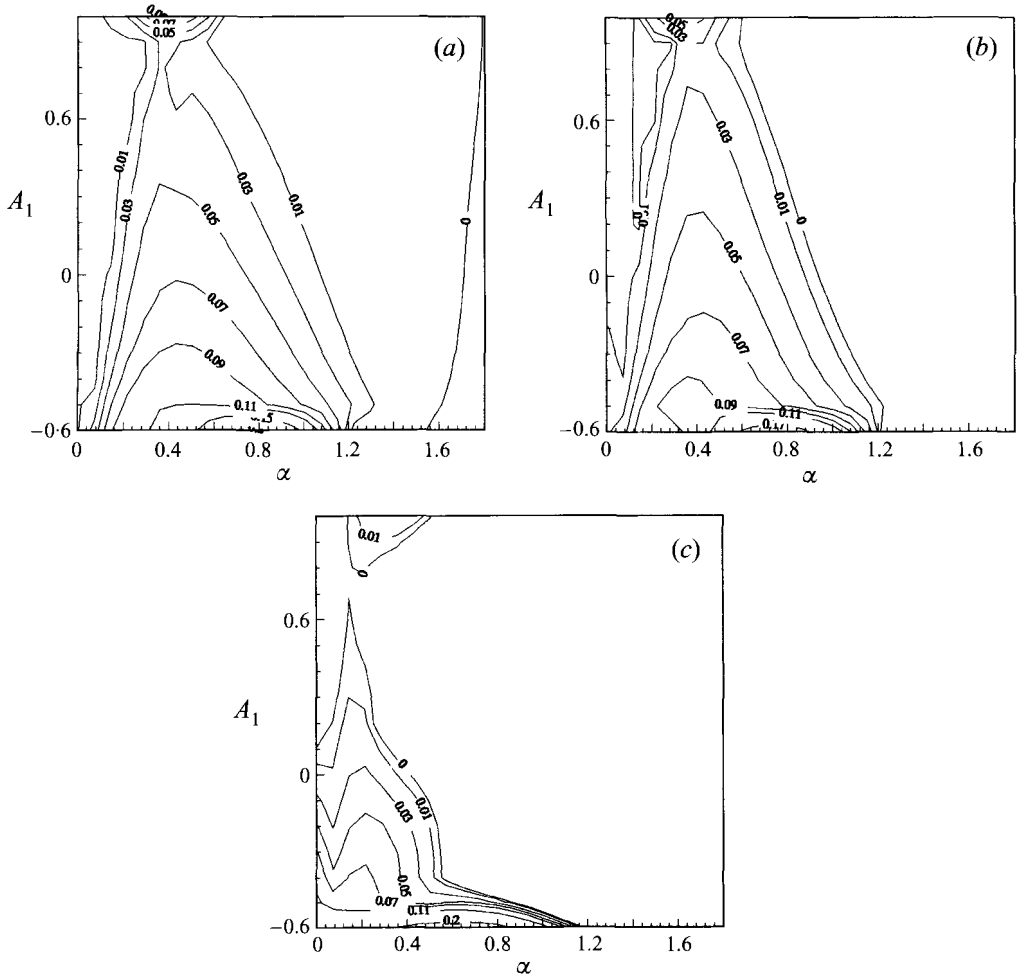


FIGURE 18. Contours of constant growth rate of the most unstable modes in the $(\alpha, A_1)$-plane for $m = 1.1$, $n = -1$, and three increasing values of $\Lambda$: 0.001 (*a*), 0.01 (*b*), and 0.1 (*c*).

effects. However, it is found here that viscous unstable modes appear only for Type II solutions, mainly for $A_1 < -0.4$, approximately, and values of $\alpha$ between 0.2 and 1.2 (see figures 16–18), so that the discrepancies may be due to the same reasons given above for the inviscid axisymmetric disturbances. Properly speaking, these viscous unstable modes appear only for disturbances with $n = -1$. For $n \geqslant 0$ viscosity does not have a significant damping effect on the inviscid instabilities with parameters in the range of the $(\alpha, A_1)$-plane just mentioned.

The map of instabilities, both inviscid and viscous, found for the cases $m = 1.2$ and $m = 1.1$ are very similar to that for $m = 1$ in terms of $A_1$ (the axial velocity at the axis). However, there exists an important difference in the physical parameter characterizing the different solutions and, therefore, their stability, which for $m \neq 1$ is a swirl parameter ($L$), precisely the one known to govern the real problem, while this is not the case in the highly degenerate case $m = 1$ (see FFB). The minor differences between $m = 1$ and $m$ slightly larger than unity occur mainly in the newly found inviscid unstable modes for axisymmetric disturbances and viscous unstable modes, both affecting only Type II solutions. It is found that for $m = 1.1$ and $m = 1.2$ these

instabilities make a sharper distinction between Type I and Type II solutions than for Long's vortex.

One of the original objectives of this work was to find if a relation exists between the solution breakdown of the model flow and its stability. That is, given the fact that vortex core solutions do not exist above a critical or folding value of the swirl parameter $L^*(m)$ (for $1 < m < 2$, which are the most relevant cases), one questions the stability of the vortices as $L$ approaches its critical value. This question is of interest in relation to the vortex breakdown phenomenon because the loss of a solution to the near-axis boundary layer equations is one of the theories proposed to explain the phenomenon (e.g. Hall 1972). In addition, it is shown elsewhere (Fernandez Feria, Fernandez de la Mora & Barrero 1996, and Perez-Saborid *et al.* 1996) that the present viscous vortex cores constitute the near-axis flow of a family of nearly inviscid conical vortices, whose structure changes abruptly to a two-cell configuration, resembling the bubble structure found in vortex breakdown, when solution breakdown of the near-axis flow occurs (see also Shtern & Hussain 1993 for the case $m = 1$). Therefore, any relation between solution breakdown of the present family of self-similar vortex cores and their stability would support another proposed explanation of the vortex breakdown phenomenon which links it to hydrodynamic instabilities (e.g. Lessen *et al.* 1974). A recent attempt in this direction was made by Gelfgat *et al.* (1996), who considered the stability of a confined swirling flow in a cylinder produced by the rotation of its base. Numerically it is found that a bubble form of vortex breakdown is reached above a critical Reynolds number (Lopez 1990). Gelfgat *et al.* found that this critical Reynolds number for vortex breakdown is smaller than the critical Reynolds number they computed for instability, concluding that vortex breakdown is not an effect of linear instability. A different conclusion was however drawn recently by Rusak & Wang (1995) in relation to the inviscid rotating flow in a pipe.

In the problem considered here it is found that all solutions, for any value of $A_1$, are unstable, at least for non-axisymmetric disturbances with $n < 0$ (this has been known for Long's vortex since the work by Foster & Duck 1982). Whence, the question is whether the growth rate of at least one type of perturbation reaches a maximum as $L \to L^*$ ($A_1 \to A_1^*$, either for Type I or for Type II solutions). In view of the present results the answer to this question is negative. Nothing particular happens to the linear stability of the present model vortex cores as the swirl parameter corresponding to the folding of Type I and Type II solutions is reached (or the folding axial flow force in the case $m = 1$). Therefore, solution breakdown (vortex breakdown) of the present vortex cores is not a consequence of linear instability. However, a significant new result is given here in relation to previous works on the stability of Long's vortex, which extends also to $m > 1$. Some new instabilities are found which affect only Type II solutions: inviscid axisymmetric instabilities, and viscous instabilities, both axisymmetric and non-axisymmetric. Of special interest are the axisymmetric modes because in most cases vortex breakdown produces an axisymmetric recirculation bubble (at least initially). In any case, it is found here that there exist instabilities which differentiate Type I and Type II solutions. Thus, one may postulate that, for the most interesting case of $m$ larger than unity, if $L$ is smaller than the folding value $L^*(m)$, the flow adopts a form corresponding to a Type I solution because Type II solutions are unstable under axisymmetric disturbances. (For non-axisymmetric disturbances both types of solutions are unstable, but one may conjecture that these instabilities saturate at small amplitude in order to preserve the generally axisymmetric character of the flow.) For increasing swirl intensity, when $L$ becomes larger than $L^*$, vortex breakdown occurs, a phenomenon which is

not related to linear instabilities. The structure of the flow then jumps to another configuration, Type III solution, which cannot be described by the near-axis boundary layer approximation used to describe the vortex cores analysed here (e.g. Beran & Culik 1992). For high-Reynolds-number flows with conical symmetry, the structure of this Type III flow is described by a two-cell conical solution (see Perez-Saborid *et al.* 1995; and Shtern & Hussain 1993 for the particular case $m = 1$). As a final comment, it seems clear from this work that to gain further insight into the phenomenon one has to consider the nonlinear (non-parallel) stability problem.

This work has been supported by the Dirección General de Investigación Científica y Técnica of Spain, Grant PB93-0974, and by a NATO Collaborative Research Grant, CRG 950368. Constant discussions with Professors J. Fernandez de la Mora and A. Barrero have been most stimulating. I am greatly indebted to both of them. I also gratefully acknowledge several comments by Profesors A. Castellanos and I. G. Loscertales.

## REFERENCES

Ardalan, K., Draper, K. & Foster, M. R. 1995 Instabilities of the Type I Long's vortex at large flow force. *Phys. Fluids* **7**, 365–373.

Batchelor, G. K. 1964 Axial flow in trailing line vortices. *J. Fluid Mech.* **20**, 645–658.

Batchelor, G. K. & Gill, A. E. 1962 Analysis of the stability of axisymmetric jets. *J. Fluid Mech.* **14**, 529–551.

Beran, P. S. & Culik, F. E. C. 1992 The role of non-uniqueness in the development of vortex breakdown in tubes. *J. Fluid Mech.* **242**, 491–527.

Burggraf, O. R. & Foster, M. R. 1977 Continuation and breakdown in tornado-like vortices. *J. Fluid Mech.* **80**, 685–703.

Cotton, F. W. & Salwen, H. 1981 Linear stability of rotating Hagen-Poseuille flow. *J. Fluid Mech.* **108**, 101–125.

Drazin, P. G., Banks, W. H. H. & Zaturska, M. B. 1995 The development of Long's vortex. *J. Fluid Mech.* **286**, 359–377.

Duck, P. W. 1986 The inviscid instability of swirling flows: large wave number disturbances. *Z. Angew. Math. Phys.* **37**, 340–360.

Duck, P. W. & Foster, M. R. 1980 The inviscid stability of a trailing line vortex. *Z. Angew. Math. Phys.* **31**, 524–532.

Duck, P. W. & Khorrami, M. R. 1992 A note on the effects of viscosity on the stability of a trailing-line vortex. *J. Fluid. Mech.* **245**, 175–189.

Escudier, M. P. 1988 Vortex breakdown: observations and explanations. In *Prog. Aero. Sci.* **25**, 189–229.

Fernandez-Feria, R., Fernandez de la Mora, J. & Barrero, A. 1995 Solution breakdown in a family of self-similar nearly-inviscid axisymmetric vortices. *J. Fluid Mech.* **305**, 77-91. (referred herein as FFB).

Fernandez-Feria, R., Fernandez de la Mora, J. & Barrero, A. 1996 Conically similar swirling flows at high Reynolds numbers. Part 1. One-cell solutions. *J. Fluid Mech.* (submitted).

Foster, M. R. 1993 Nonaxisymmetric instability in slowly swirling jet flows. *Phys. Fluids* **5**, 3122–3135.

Foster, M. R. & Duck, P. W. 1982 The inviscid stability of Long's vortex. *Phys. Fluids* **25**, 1715–1718.

Foster, M. R. & Jacqmin, D. 1992 Non-parallel effects in the stability of Long's vortex. *J. Fluid Mech.* **244**, 289–306.

Foster, M. R. & Smith, F. T. 1989 Stability of Long's vortex at large flow force. *J. Fluid Mech.* **206**, 405–432.

Gelfgat, A., Bar-Yoseph, P. & Solan, A. 1996 Stability of confined swirling flow with and without vortex breakdown. *J. Fluid Mech.* **311**, 1–36.

Hall, M. G. 1972 Vortex breakdown. *Ann. Rev. Fluid Mech.* **4**, 195–218.

HOWARD, L. N. & GUPTA, A. S. 1962 On the hydrodynamic and hydromagnetic stability of swirling flows. *J. Fluid Mech.* **14**, 463–476.

KHORRAMI, M. R. 1991*a* On the viscous modes of instability of a trailing line vortex. *J. Fluid Mech.* **225**, 197–212.

KHORRAMI, M. R. 1991*b* A Chebyshev spectral collocation method using a staggered grid for the stability of cylindrical flows. *Intl J. Num. Methods Fluids* **12**, 825–833.

KHORRAMI, M. R. 1992 Behaviour of asymmetric unstable modes of trailing line vortex near the upper neutral curve. *Phys. Fluids* A **4**, 1310–1313.

KHORRAMI, M. R. & TRIVEDI, P. 1994 The viscous stability analysis of Long's vortex. *Phys. Fluids* **6**, 2623–2630 (referred herein as KT).

LEIBOVICH, S. 1984 Vortex stability and breakdown: survey and extension. *AIAA J.* **22**, 1192–1206.

LEIBOVICH, S. & STEWARTSON, K. 1983 A sufficient condition for the instability of columnar vortices. *J. Fluid Mech.* **126**, 335–356.

LESSEN, M. & PAILLET, F. 1974 The stability of a trailing line vortex. Part 2. Viscous theory. *J. Fluid Mech.* **65**, 769–779.

LESSEN, M., SINGH, P. J. & PAILLET, F. 1974 The stability of a trailing line vortex. Part 1. Inviscid theory. *J. Fluid Mech.* **63**, 753–763.

LONG, R. L. 1958 Vortex motion in a viscous fluid. *J. Met.* **15**, 108–112.

LONG, R. L. 1961 A vortex in an infinite fluid. *J. Fluid Mech.* **11**, 611–625.

LOPEZ, J. M. 1990 Axisymmetrical vortex breakdown. Part 1. Confined swirling flow. *J. Fluid Mech.* **221**, 533–552.

MAYER, E. W. & POWELL, K. G. 1992 Viscous and inviscid instabilities of a trailing vortex. *J. Fluid Mech.* **245**, 91–114.

OGAWA, A. 1993 *Vortex Flows.* CRC Press.

PEREZ-SABORID, M., BARRERO, A., FERNANDEZ-FERIA, R. & FERNANDEZ DE LA MORA, J. 1996 Conically similar swirling flows at high Reynolds numbers. Part 2. Two-cell solutions. *J. Fluid Mech.* (submitted).

RUSAK, Z. & WANG, S. 1995 A theory of the axisymmetric vortex breakdown. *Bull. Am. Phys. Soc.* **40**, 2044.

SHTERN, V. N. & HUSSAIN, F. 1993 Hysteresys in a swirling jet as a model tornado. *Phys. Fluids* A **5**, 2183–2195.

SPALL, R. E., GATSKI, T. B. & GROSCH, C. E. 1987 A criterion for vortex breakdown. *Phys. Fluids* **30**, 3434–3440.

STEWARTSON, K. 1982 The stability of swirling flows at large Reynolds number when subjected to disturbances with large azimuthal wave number. *Phys. Fluids* **25**, 1953–1957.

UBEROI, M. S., CHOW, C. Y. & NARAIN, J. P. 1972 Stability of coaxial rotating jet and vortex of different densities. *Phys. Fluids* **15**, 1718–1727.